Available online at www.sciencedirect.com

ScienceDirect

Underground Space 26 (2026) 364–386

www.keaipublishing.com/undsp

Research Paper

Experimental study on rock damage and failure induced by multi-source dynamic disturbances

Han-Yi Liu, Ben-Guo He *, Jia-Hua Guan, Hong-Yuan Fu

Key Laboratory of Ministry of Education on Safe Mining of Deep Metal Mines, Northeastern University, Shenyang 110819, China

Received 8 April 2025; received in revised form 20 August 2025; accepted 21 September 2025
Available online 4 December 2025

Abstract

Research into the mechanical behaviour of rock surrounding the deep-buried tunnel under multi-source dynamic disturbance is key to the safety of underground engineering operations. Based on a dynamic true-triaxial testing apparatus, the present study examined the mechanical behaviours and fracture mechanisms of deep granite under the coupled effects of intermediate-frequency dynamic disturbance ($f = 300$ Hz) and low-frequency dynamic disturbance ($f = 5$–20 Hz). Intermediate-frequency dynamic disturbance markedly initiates the genesis of tensile micro-cracks within rock, while low-frequency dynamic disturbance exacerbates the propagation and interconnection of cracks, ultimately leading to the formation of a tensile-shear mixed failure mode. The severity of the influence of intermediate-frequency disturbance on the peak strength of rock is the initial crack compaction σ_{cc} (decreased by 8.1%), the damage stress σ_{cd} (decreased by 6.4%), and the crack initiation stress σ_{ci} (decreased by 4.7%) under different disturbance timings. This changes the characteristic stress of the rock and significantly decreases its brittleness index. Meanwhile, the low-frequency f of weak disturbance significantly affects the failure mode and peak strength of the rock. The peak strength σ_p exhibits U-shaped variation, with the maximum decrease reaching 15 MPa, which indicates the presence of a resonance effect between the external disturbance and the natural frequency of the rock. The timing of intermediate-frequency disturbance alters the natural frequency of the rock. Analysis of the fracture surface shows that cracks induced by intermediate-frequency disturbance primarily propagate along the σ_1-direction, while low-frequency disturbance promotes propagation of shearing cracks along the σ_3-direction. Brittle failure occurs due to the through-going shearing cracks. The results further reveal the synergistic mechanism of action of multi-source dynamic disturbance on rock failure, indicating that the coupled effects of multi-source dynamic disturbances significantly increase the risk of brittle failure in the rock mass.

Keywords: True-triaxial compression; Dynamic disturbance; Tensile-shear failure; Characteristic stress; Resonance effect

1 Introduction

Deep-buried tunnels undergo extremely complex in-situ stress environments during excavation (Zhang et al., 2012). Besides the instantaneous loading and unloading effects caused by ultra-high excavation stresses (Li et al., 2014), rock surrounding the tunnel is also affected by multi-source dynamic disturbances (Xie et al., 2020), including intermediate-frequency disturbance stresses from drilling and blasting (D&B) methods and sustained low-frequency vibrations from tunnel boring machine (TBM) operations (Liu et al., 2022), as well as complex stress wave effects from geological events such as earthquakes and rockbursts. These dynamic sources exhibit different frequency (f) and amplitude (A) characteristics, and their interactions and superimposed effects further complicate the dynamic responses of rock surrounding the tunnel. The intermediate-frequency disturbance waves induced by D&B methods exhibit intense and short-duration impacts on the hard rock (Scoble et al., 1996), while TBM operations lead to cumulative damage through sustained low-frequency vibrations. More critically, intermediate-

* Corresponding author.
E-mail address: hebenguo@mail.neu.edu.cn (B.-G. He).
Peer review under the responsibility of Tongji University

https://doi.org/10.1016/j.undsp.2025.09.003

frequency and high-amplitude stress waves from geological disasters such as earthquakes and rockbursts can cause pre-damage to rock surrounding the tunnel, forming tensile cracks and significantly decreasing the loading capacity of the rock (Waqar et al., 2023). These tensile cracks continue to develop, leading to brittle failure characterized by an instantaneous shearing crack through-going under subsequent high excavation stress and low-frequency dynamic disturbances (Lamert et al., 2018), which induces instability of the rock surrounding tunnels and violent rockbursts. This type of rockburst is distinguished by tensile-shear failure at the burst boundary (Feng et al., 2023, 2012).

Research into the dynamic mechanical properties of deep-buried hard rock relies on laboratory experiments, while the high and low-frequency disturbances have been investigated as relatively independent research directions (Zhang et al., 2014). Studies on high-frequency disturbances utilised the Split-Hopkinson Pressure Bar (SHPB) apparatus, which simulates the extremely high-frequency disturbance conditions common in deep engineering (Zhou et al., 2010). Experimental results indicate that hard rock subjected to high-frequency disturbances exhibits pronounced brittle failure (Luo et al., 2025), with failure strength closely related to loading rate (Mishra et al., 2017) and strain rate (Mishra et al., 2018). However, these results are often based on extremely high-frequency impact waves, which may not fully represent the frequency and amplitude ranges experienced by rocks in an actual deep engineering environment (Xie et al., 2022). Deep engineering typically involves intermediate to lower-frequency dynamic disturbances (Peng et al., 2019), making it challenging to apply SHPB results directly to real engineering construction. In addition, the design of SHPB test emphasises the failure strength and fracture mode of rock, and brittle failure often occurs under impact load during the test (Majedi et al., 2020). This limits SHPB data to the study of the dynamic response of rock in undamaged states, such as those involving elasto-plastic deformation. In fact, rock subjected to strong disturbance may not completely fail in many engineering applications, especially in the case of dynamic disturbance with low strain and loading rate.

In contrast, low-frequency disturbances are often investigated using dynamic true-triaxial tests (Su et al., 2017), which can apply continuous and repeated low-frequency loading to simulate the dynamic disturbance influence of excavation, tunnelling, and other long-term operational disturbances (Dai et al., 2023). The true triaxial dynamic test can be used to investigate the peak strength (σ_p), peak strain (ε_p), failure characteristics, and mechanism underpinning the energy evolution of rock under low-frequency dynamic disturbances (He et al., 2023). Low-frequency disturbances significantly influence the plastic deformation (Eberhardt et al., 1999), micro-crack propagation, and failure modes of rock, with cumulative damage from repeated loads gradually decreasing the σ_p and energy storage capacity of the rock (Jiang et al., 2021).

They are manifested in the isolated study of the mechanical properties of hard rock under two stress conditions: intermediate-frequency strong disturbance and low-frequency repeated dynamic disturbance. This may neglect the coupled effects of multi-source dynamic disturbances. Intermediate and low-frequency disturbances often coexist and interact during the excavation process, potentially exacerbating the damage to the rock (Falls et al., 1998). Intermediate-frequency disturbances may induce tensile crack propagation or localised damage within the rock before stress concentration, which will significantly change its mechanical response to low-frequency disturbance. The coupled effects of intermediate and low-frequency dynamic disturbances on the mechanical properties of rock remain a critical issue in rock mechanics. The influence of dynamic disturbance at different frequencies on rock has obvious spatial–temporal characteristics (disturbance timing and direction). The true triaxial mechanical test of rock will be carried out to investigate these coupled effects, which is essential for accurate investigation of rock failure mechanisms and stability under complex dynamic conditions. The results can provide theoretical guidance for the design and safety evaluation of deep-buried tunnels.

2 Engineering background and experimental work

2.1 Testing apparatus

The testing apparatus is a dynamic true-triaxial experimental system independently developed by Northeastern University, China (Fig. 1(a)) (Feng et al., 2023). The system can simultaneously apply three principal stress directions (X, Y, Z). Weak dynamic disturbance stress can be applied in the Z-direction, with a maximum dynamic disturbance frequency of 40 Hz. The intermediate-frequency disturbance stress is applied by an independently equipped intermediate-frequency slow-wave dynamic disturbance bar (Fig. 1(b)). The intermediate-frequency dynamic disturbance can be applied in the σ_1-direction on the specimens, and the disturbance amplitude A = 0–30 MPa is controlled by the bullet launch pressure. The disturbance rod is equipped with six different bullet lengths (2.60, 2.88, 3.25, 3.72, 4.33, and 13.33 m). Therefore, the dynamic disturbance frequency can be realised at f = 500, 450, 400, 350, 300, and 100 Hz, respectively (Xia et al., 2015), to cover the intermediate-frequency disturbance frequency range subjected to deep-buried hard rock (Fig. 1(c)).

2.2 Engineering background and the stress path

During the TBM excavation of a deep-buried tunnel in south-western China, a strong rockburst occurred at the arched crown of the tunnel (Fig. 2). It is found that there have been many earthquakes in this area, and seismic waves will produce intermediate-frequency dynamic disturbance effects acting in the tangential direction of the tunnel. Additionally, the D&B method was used to construct the

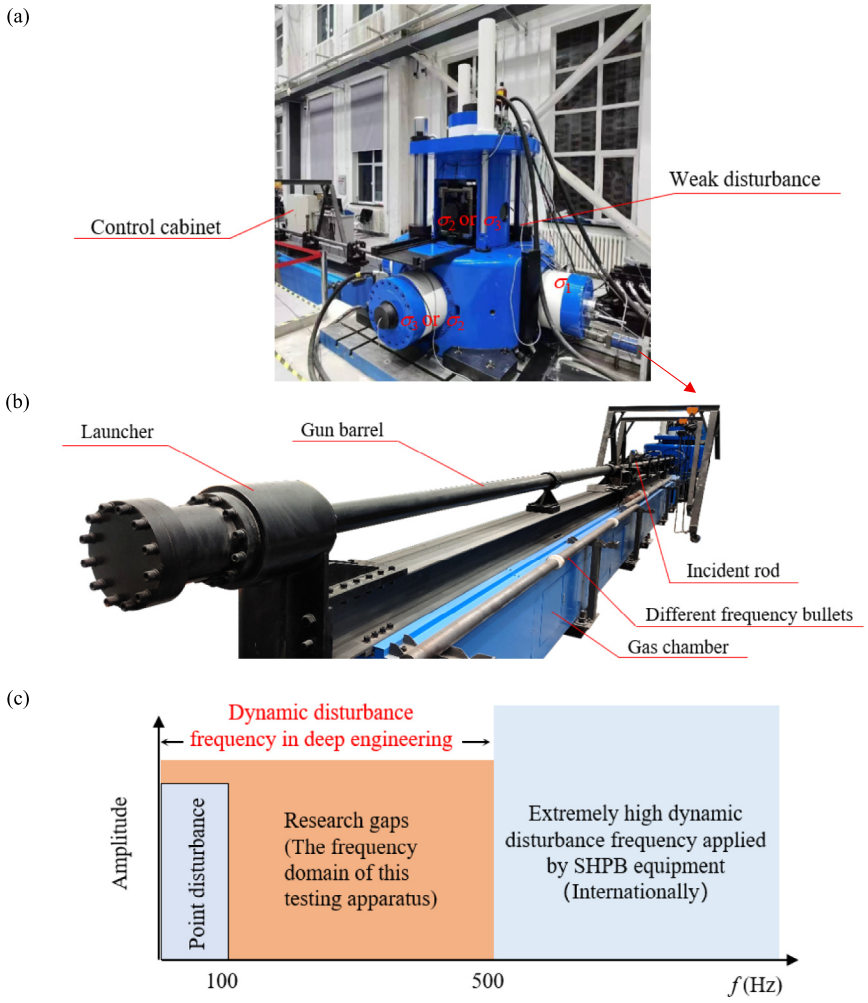

Fig. 1. True triaxial hard rock intermediate and low-frequency dynamic disturbance coupled loading testing apparatus. (a) Low-frequency dynamic disturbance testing apparatus, (b) intermediate-frequency and slow-wave disturbance rod, and (c) deep engineering frequency range. The apparatus can apply intermediate-frequency (f = 0–500 Hz) disturbance stress.

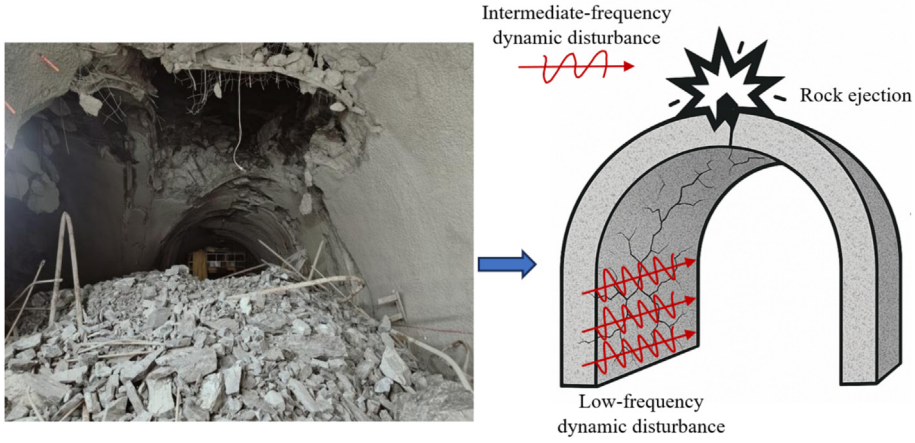

Fig. 2. Strong rockburst occurred at the crown of an arch in a deep-buried tunnel.

transverse hole, which also produced dynamic disturbance in the process of excavation in the tunnel. Finally, the low-frequency dynamic disturbance generated during TBM tunnelling continues to trigger rockburst. Although intermediate-frequency disturbances are characterized by larger amplitude A, the rock mass, being under a true-

triaxial stress state with high strength, does not fracture immediately. Instead, it gradually accumulates energy through elastic–plastic deformation. Subsequently, continuous and repeated exposure to low-frequency dynamic perturbations fosters an accumulation of stress within the rock mass, progressively encouraging the convergence of internal fractures until they culminate in catastrophic brittle failure.

A schematic diagram of adjacent tunnel excavation under TBM construction was plotted in Fig. 3(a). The intermediate-frequency dynamic disturbance stress generated during the excavation of working face II is transmitted to the arched crown of the adjacent tunnel, while the low-frequency disturbance caused by the TBM excavation at working face I is transmitted in the form of continuous and repeated dynamic disturbances along the tunnel axis to the rock surrounding behind the working face. In this process, the intermediate-frequency disturbance transmitted from the adjacent tunnel propagates along the tangential direction of the tunnel, corresponding to σ_1-direction. In contrast, the low-frequency disturbance propagates along the tunnel axis, clearly corresponding to σ_2-direction. A schematic representation of the stress paths is provided for expounding the mechanical behavior of rock surrounding the tunnel under the coupled effects of intermediate and low-frequency dynamic disturbances under true-triaxial conditions (Fig. 3(b)). It is worth noting that the intermediate-frequency dynamic disturbances are applied at specific points during the true-triaxial loading process of the specimen, namely the point of the initial crack compaction stage (σ_{cc}), the crack initiation stress point (σ_{ci}) (Ingraffea et al., 1987), and the damage stress

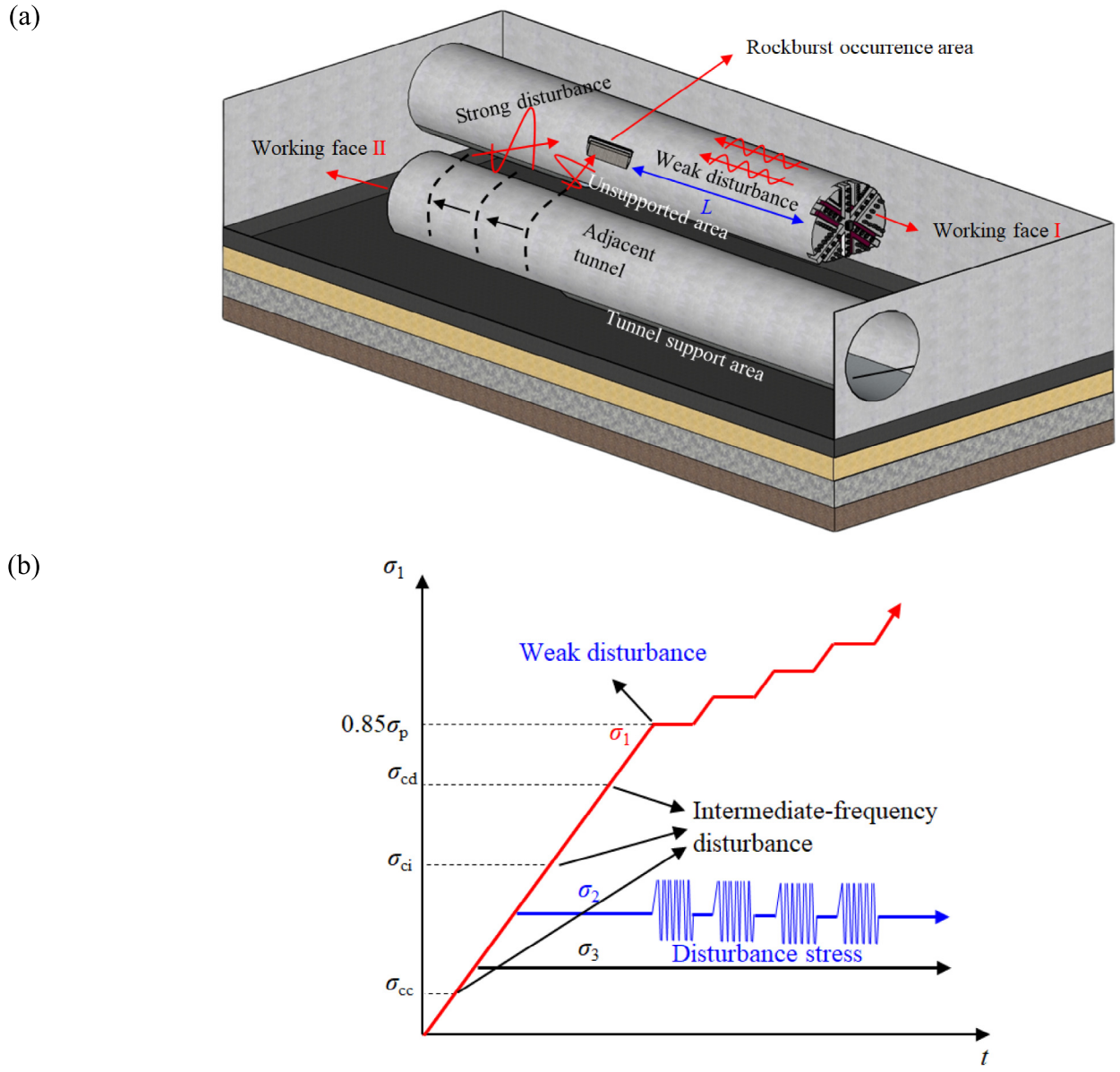

Fig. 3. Schematic diagram of weak disturbance triggering rockburst. (a) Rockburst induced by the TBM tunnelling method, and (b) intermediate-frequency disturbance and weak disturbance loading along true triaxial stress path.

point (σ_{cd}) (Bahrani et al., 2017). The unexcavated rock mass remains at the crack-closure phase in the rock surrounding deep-buried tunnels, where the inflection point of the initial crack compaction phase often corresponds to the initial in-situ stress conditions (Strickland et al., 1980). Therefore, applying intermediate-frequency dynamic disturbances to the unexcavated rock mass can be considered at the σ_{cc} point. The rock surrounding undergoes stress unloading in the radial direction (σ_3) of the tunnel after excavation, leading to stress concentration and a sudden increase in the principal stress (σ_1-direction) (Li et al., 2018). In this study, the timing of intermediate-frequency dynamic disturbances under such conditions corresponds to the crack initiation stress point (σ_{ci}) and the damage stress point (σ_{cd}). In summary, this represents the spatial–temporal effects of the coupling between intermediate and low-frequency dynamic disturbances (Qian et al., 2024).

2.3 Selection of intermediate and low-frequency dynamic disturbance frequencies

The excavation method significantly affects the dynamic disturbance sources in deep-buried tunnel engineering, primarily reflected in two excavation methods: TBM method and D&B method (Barton et al., 2012). These two excavation methods exhibit different characteristics in the dynamic disturbance frequency (f) and amplitude (A). The TBM excavation method advances continuously through mechanical cutting, generating dynamic disturbances that typically manifest as long-term vibrations. As shown in Fig. 4, the dynamic disturbance frequency-amplitude characteristics of a TBM-excavated tunnel in south-western China were measured. The low-frequency disturbance frequency associated with TBM axial direction vibrations ranged from 1 to 30 Hz, whereas higher frequencies ($f \approx 322.95$ Hz) corresponded to radial and tangential vibrations. Due to the relatively stable cutting process of the TBM, the vibrations generated are continuous in the time domain. This low-frequency dynamic disturbance tends to induce the propagation of microcracks within the rock, thereby affecting the stability of the rock surrounding such tunnels.

In contrast, the D&B tunnel advances periodically through blasting, and dynamic disturbances are primarily characterized by intermediate-frequency pulse vibrations (Ayala, 2017). The energy released during blasting propagates through adjacent rock masses in the form of

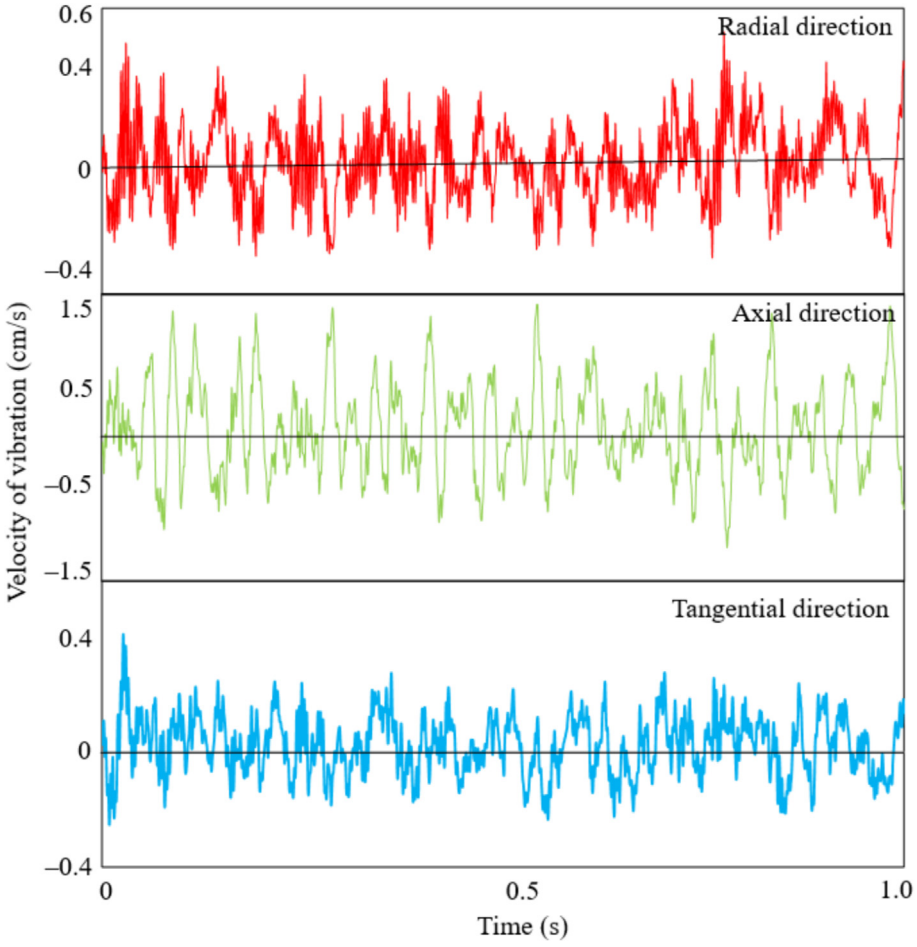

Fig. 4. Monitoring of tunnel vibration by the TBM method.

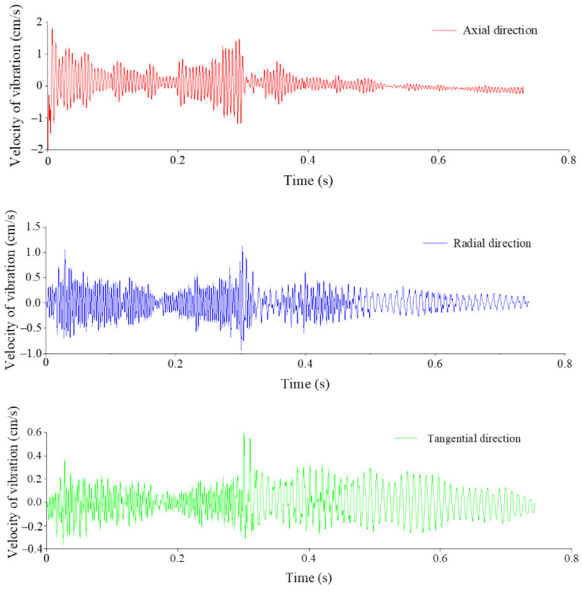

Fig. 5. Monitoring of tunnel vibration by D&B.

intermediate-frequency disturbance waves. Such intermediate-frequency disturbances exhibit strong propagation capability and an extremely short duration, potentially causing deformation of the rock within a localised spatial range. The vibration monitoring data from a tunnel constructed using the D&B method indicate a tangential direction dynamic disturbance frequency ($f \approx 318.34$ Hz) (Fig. 5). The duration of each disturbance is extremely brief, and the vibration velocity is relatively high.

2.4 Experimental and testing specimens

Dynamic true-triaxial compression tests were conducted on homogeneous deep granite to investigate the physical and mechanical properties of granite under the coupled effects of multi-source dynamic disturbances. The testing apparatus was equipped with a servo system, which can independently apply static true triaxial stresses ($\sigma_1 > \sigma_2 > \sigma_3$) to the specimen under stress control, with a loading rate of 0.5 MPa/s. Intermediate-frequency disturbances were applied to the σ_1-direction plane of the specimen via the disturbing rod. The deformation rate was set to 0.015 mm/min, and the rock specimen was further loaded to $0.85\sigma_p$ under deformation control, where low-frequency dynamic disturbances were applied thereto. Low-frequency dynamic disturbances were applied continuously and over an extended duration to the σ_2-direction of the specimen. Each loading stage maintained the dynamic disturbance for 5 min. That in the σ_1-direction was increased by 5 MPa if brittle failure did not occur during a given stage, and the dynamic disturbance was reapplied. The experimental scheme is shown in Table 1.

Figure 6 shows the waveform obtained using the intermediate-frequency disturbance stress wave regulator during the intermediate-frequency disturbance rod. When the bullet pressures are 0.15, 0.25, and 0.40 MPa, the absolute value of the corresponding strain gauge voltage gradually increases, indicating an increase in the amplitude A of the intermediate-frequency disturbance. The voltage across the strain gauge decreases first, then increases, representing the incident wave and reflected wave of the intermediate-frequency stress wave. The reflected wave is significantly lower than the incident wave, indicating that the lost energy is absorbed by the rock specimens and converted into the tensile crack for energy release. Figure 6(d) shows four groups of typical disturbance stress waves measured in experiments, and the similarity therein is consistent.

Table 1
Experimental scheme of intermediate and low-frequency coupled dynamic disturbance.

Low frequency timing	Intermediate frequency timing	Weak disturbance		Strong disturbance	
		A (MPa)	f (Hz)	A (MPa)	f (Hz)
$0.85\sigma_p$	σ_{cd}	1	5	15	300
	σ_{ci}		10		
	σ_{cc}		15		
			20		
$0.85\sigma_p$	σ_{ci}	1	20		
		3			
		5			
$0.85\sigma_p$	σ_{cd}	1	20 (σ_2)		
			20 (σ_3)		

This study selected the ultra-homogeneous deep granite as the experimental rock material to reduce the random influence of the rock homogeneity coefficient on the test results. All the specimens were derived from the same intact rock mass. Each rock specimen was marked with its upper, lower, and side directions during mining to reduce the error effect (Fig. 7). Three or five specimens were tested in each group to make the results more convincing.

3 Results and analysis

To verify the homogeneity of the granite specimens and determine the peak strength (σ_p) of granite under stress conditions of $\sigma_2 = 20$ MPa and $\sigma_3 = 5$ MPa (Fig. 8(a)), the peak strengths of the granite specimens A1, A2, and A3 were 287, 294, and 288 MPa, respectively. The average σ_p is 290 MPa, and the high overlap of the curves indicates that the granite specimens exhibit good homogeneity, with stable mechanical properties. Crack analysis method calculates the characteristic stress by crack volume ε_v^c (Scavia, 1995), including the crack initiation stress (σ_{ci}) and the damage stress (σ_{cd}), as shown in Fig. 8(b). The average values of σ_{ci} and σ_{cd} are 157 and 214 MPa, respectively, which correspond to 54% and 74% of σ_p. In addition, the elastic modulus of granite under these stress conditions is 57.7 GPa. The failure mode is shearing failure (Haimson, 2006), as shown in Fig. 8(c).

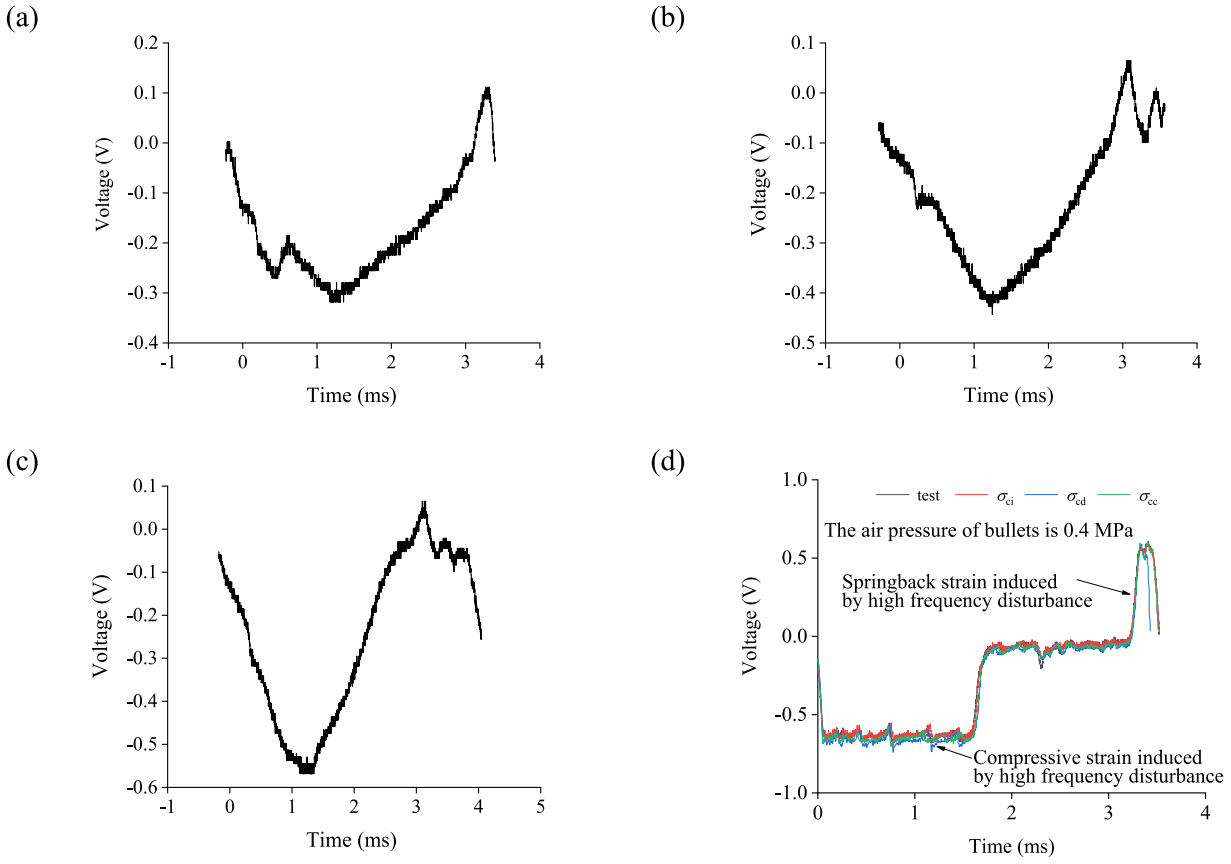

Fig. 6. Changes in the strain gauge voltage under different intermediate-frequency dynamic disturbance stresses with bullet pressures of (a) 0.15 MPa, (b) 0.25 MPa, and (c) 0.40 MPa; (d) intermediate-frequency disturbance repeated stress test at a pressure of 0.4 MPa.

Fig. 7. Granite specimens.

3.1 Mechanical properties of rock under multi-source dynamic disturbance

The stress–strain curve of granite under multi-source dynamic disturbance conditions is shown in Fig. 9. The intermediate-frequency disturbance timing applied is (a) σ_{cc}, (b) σ_{ci}, and (c) σ_{cd}. The specimen is preloaded to $0.85\sigma_p$ before applying low-frequency disturbances. At the moment of intermediate-frequency disturbance, deformation control is applied in the σ_1-direction. Due to the intermediate-frequency disturbance, the specimen undergoes instantaneous compressive deformation in the σ_1-direction. Once the deformation servo-motor control system detects this information, the instantaneous stress is adjusted to the stress level corresponding to the strain. The reduced stress amplitude can then be considered as the instantaneous stress generated during this intermediate-frequency disturbance. The mean value of the disturbance stress is $A = 15$ MPa. The σ_p values of granite under the influences of three different intermediate-frequency disturbance timings are 271.5, 266.5, and 266.5 MPa, respectively. The average σ_p is decreased by 7.5%, which is greater than the effect of a single low-frequency disturbance source applied in the σ_2-direction. The primary effect of multi-source dynamic disturbance is manifested in the failure mode of the rock. Due to the influence of intermediate-frequency disturbance, independent tensile cracks are initiated in the σ_1-direction, but no through-going fractures are formed. Subsequently, the cracks gradually propagate and form through-fractures under the influence of low-frequency disturbance in the σ_2-direction, manifest by the connection and expansion of tensile cracks within the rock. The internal stress field of the rock changes, leading to a shift in the direction of crack propagation from the σ_1-direction to the

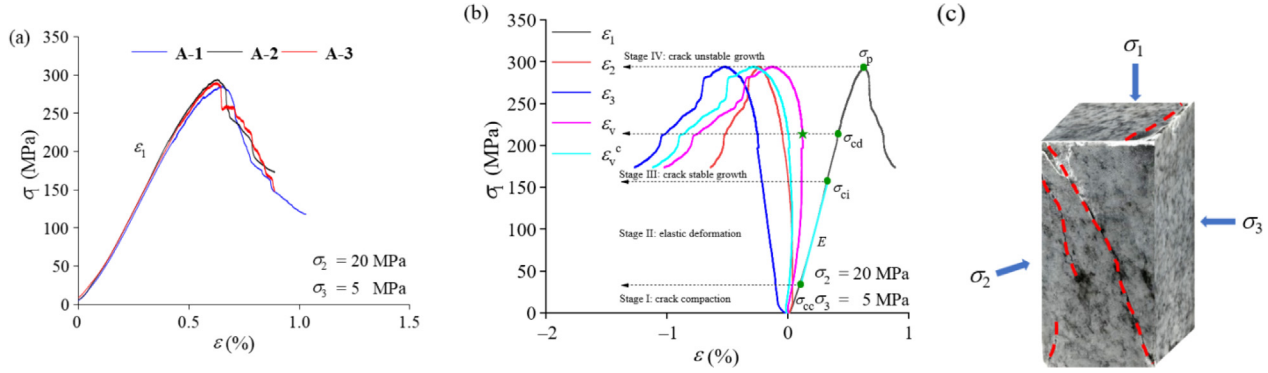

Fig. 8. Peak strength (σ_p) comparison and characteristic stress. (a) Excellent coincidence of post-peak curves, (b) characteristic stress, and (c) failure mode.

σ_3-direction under the influence of low-frequency disturbance. This process is accompanied by the redistribution of stress concentration areas within the rock and a transition in crack morphology. Ultimately, the rock exhibits a complex failure mode with crack propagation influenced by multi-source dynamic disturbance.

3.2 Influences of different low-frequency disturbance frequencies

The true triaxial stress–strain curves under intermediate-frequency disturbance point σ_{cc} and low-frequency disturbance frequencies of 5, 10, 15, and 20 Hz are presented in Fig. 10(a). The σ_p values of the rock are 261.5, 261.5, 271.5, and 271.5 MPa, with a maximum decrease of 9.8%, and an average σ_p of 266.5 MPa. The failure mode exhibits multiple tensile-shear mixed zones, which result from intermediate-frequency disturbance generating tensile cracks at the ends due to local stress concentration after the compressive dense segment ends. Low-frequency disturbance, on the other hand, promotes crack propagation and through-crack formation, altering the distribution of the internal stress field in the rock. Low-frequency disturbance enhances the connectivity of the cracks, causing localised cracks to develop into through-cracks. The synergistic effect of the two disturbance frequencies accelerates the fracture process of the rock, revealing the non-linear characteristics of multi-source dynamic disturbance on the mechanism of rock failure, which is not a simple coupling or superposition effect. It is noteworthy that obvious shear cracks appear in the σ_3-plane of the specimen, and the cracks even take on a through form at $f = 5$ Hz and 10 Hz. This is a typical feature generated by the intermediate-frequency disturbance at the σ_{cc} point. The reason is that the intermediate-frequency disturbance occurring at this point causes instantaneous oscillations in the internal crystalline lattice of the rock; this is accompanied by the rapid expansion and aggregation of internal microcracks as σ_1 increases, leading to the formation of through-cracks in the σ_3-plane as well. This intermediate-frequency disturbance timing induces initial damage (tensile micro-cracks) in the intact rock specimen, hence the reduction in its peak strength.

Similarly, the true triaxial stress–strain curves under intermediate-frequency disturbance point σ_{ci} and low-frequency disturbance frequencies of 5, 10, 15, and 20 Hz are shown in Fig. 11(a). The values of σ_p of the rock are 276.5, 281.5, 281.5, and 266.5 MPa, respectively. σ_p decreases by a maximum of 8.1% when $f = 20$ Hz, but the average strength reaches 276.5 MPa, which is higher than that of the specimen with the disturbance point σ_{cc}. The failure mode still exhibits complex tensile-shear mixed failure. The difference lies in the significantly reduced length and number of surface tensile cracks, but multiple instances of rock fragment spalling occur at the ends of the specimens. In addition, non-through tensile cracks can be observed except for $f = 15$ Hz in the σ_3-plane of the specimen. It can be observed that the higher the peak strength of the rock specimen, the greater the degree of fragmentation, which indicates that the low-frequency disturbance frequency affects the connection and propagation of tensile microcracks within the rock.

Finally, the triaxial stress–strain curves under intermediate-frequency disturbance point σ_{cd} and low-frequency disturbance frequencies of 5, 10, 15, and 20 Hz are presented in Fig. 12(a). The σ_p of the rock are 266.5, 276.5, 276.5, and 266.5 MPa, with a maximum decrease of 8.1% at $f = 5$ Hz and 20 Hz. The average peak strength is 271.5 MPa. As the dynamic disturbance frequency increases, the tensile cracks on the rock failure surface become more pronounced, and the tensile-shear mixed failure becomes more evident, leading to a decrease in σ_p.

In summary, the importance of the influences of different intermediate-frequency disturbance timings can be obtained as follows: $\sigma_{cc} > \sigma_{cd} > \sigma_{ci}$ (Fig. 13(a)). The influence of intermediate-frequency disturbance timing on rock mechanics was investigated from the perspective of the macroscopic fracture surface. It can be concluded that rock subjected to intermediate-frequency disturbance at the σ_{cc} point is accompanied by more primary fractures. As a result, this intermediate-frequency disturbance timing leads to the largest tensile region. The failure surface is not only confined to the σ_2-direction but also exhibits almost complete through-cracks on the σ_3-direction surface. These factors can explain the reasons for the greater damage caused to the rock by intermediate-frequency disturbance at this

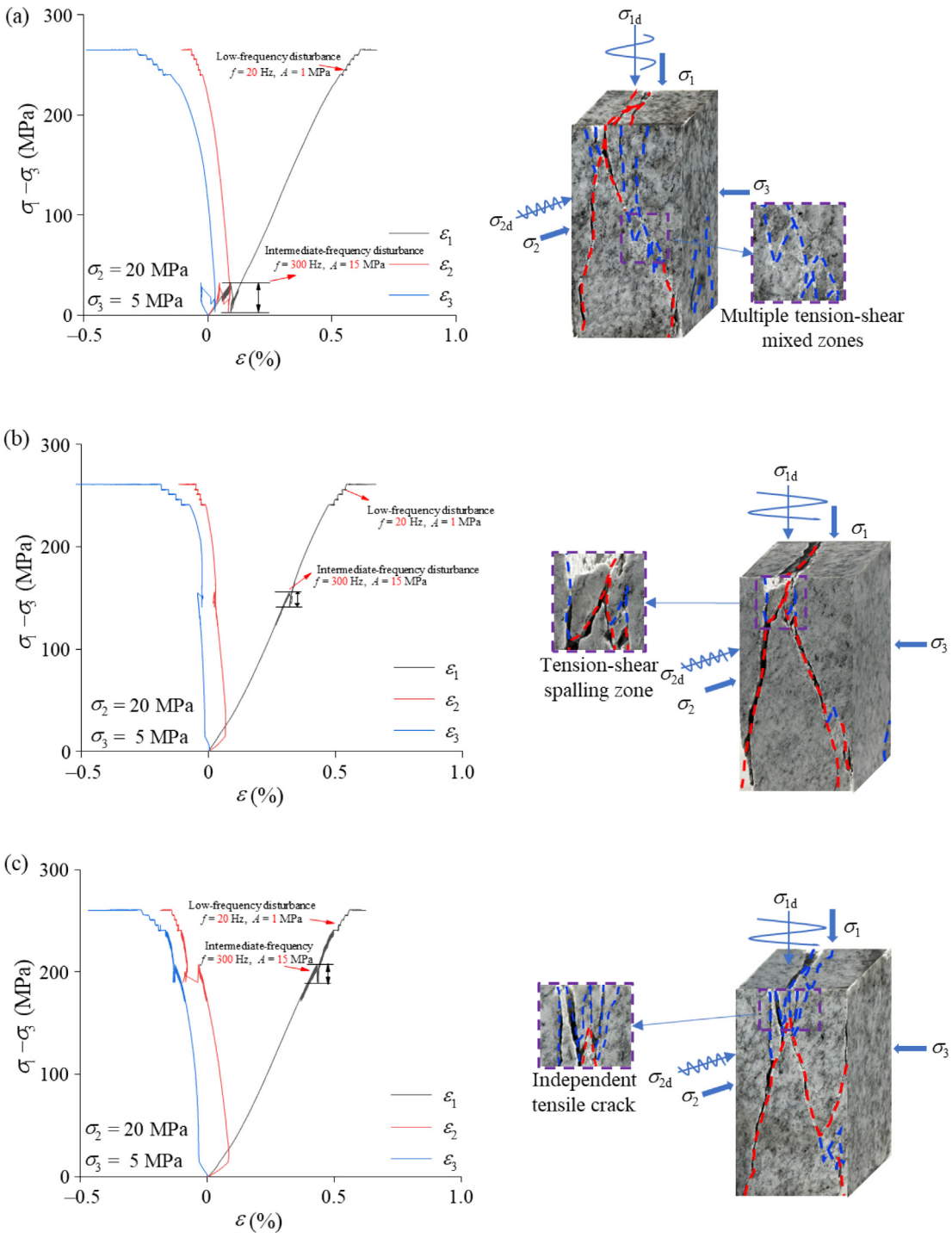

Fig. 9. True triaxial complete stress–strain curves under different intermediate-frequency disturbance timings. (a) σ_{cc}, (b) σ_{ci}, and (c) σ_{cd}. Three different intermediate-frequency disturbance timings bring about different crack morphologies in the tensile-shear zone.

point. The greater impact of intermediate-frequency disturbance at the σ_{cd} point compared to the σ_{ci} point is more straightforward. That is, the rock has already reached the inflection point of volumetric strain at the crack damage phase, and damage has occurred within the specimen. In contrast to the crack initiation stage, there are more microfractures within the specimen. These microfractures will continue to develop under the influence of intermediate-frequency disturbance, leading to a significant decrease in σ_p of the rock.

Regarding the aspect of the influence of low-frequency dynamic disturbance, the variation in σ_p is U-shaped with increasing disturbance frequency. This behaviour is related to the natural frequency of the rock specimen. When the

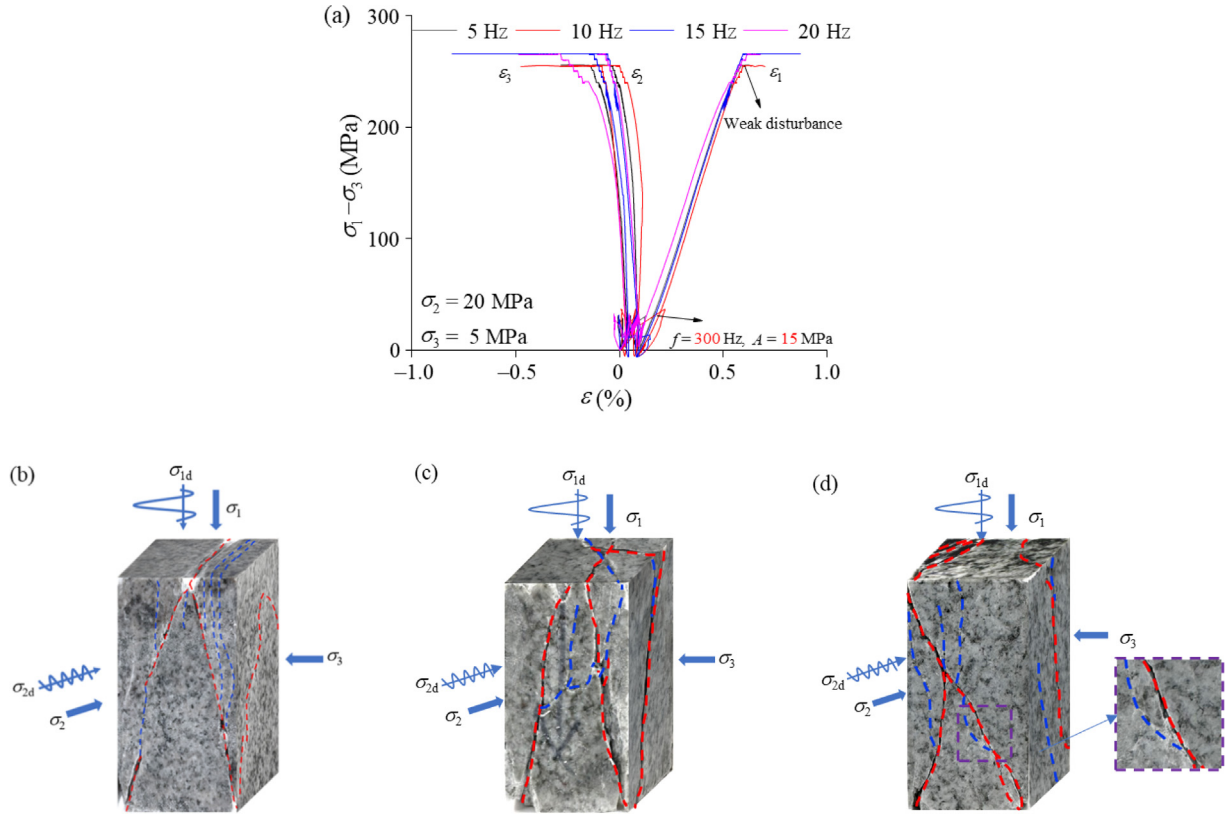

Fig. 10. Influences of different weak disturbance frequencies on the disturbance at the σ_{cc} point with (a) σ_1 comparison, and the failure mode with low-frequency of (b) 5 Hz, (c) 10 Hz, and (d) 15 Hz, and Fig. 9(a) 20 Hz. Longer tensile cracks are clearly visible and more cracks appear in the σ_3-direction, which may be the reason for the decrease in σ_1.

external loading frequency coincides with the rock's natural frequency under the true triaxial stress condition, a significant decrease in σ_p of the rocks occurs. The natural frequencies of the specimens with intermediate-frequency disturbance at σ_{ci} and σ_{cd} are about 15–20 Hz, while the natural frequency of the specimen with intermediate-frequency disturbance at σ_{cc} may appear in the range of 5–10 Hz.

In terms of peak strain (Fig. 13(b)), granite specimens under different intermediate and low-frequency disturbance frequencies all show a decreasing trend inε_3 that affects failure, within their respective natural frequency ranges. This is by no means a coincidental phenomenon that indicates the significant influence of the natural frequency range on the deformation of the rock in the σ_3-direction. This could be the main reason why natural frequency affects the σ_p of the rock.

Finally, statistical analysis shows that the fracture angle of the rock is generally inversely proportional to its σ_p from the perspective of rock fracture (Fig. 13(c)). The larger the fracture angle, the more the macroscopic cracks tend to exhibit tensile fracture. The specimens at σ_{cc} under intermediate-frequency disturbance exhibit the largest fracture angle among them, indicating that this intermediate-frequency disturbance generates the largest number of tensile cracks, severely affecting the failure of the rock and its peak strength.

3.3 Characteristic stress and brittleness index

Crack volume was calculated using crack analysis methods, and the crack strain and volumetric strain at a low-frequency disturbance of $f = 5$ Hz were determined for different intermediate-frequency disturbance timings through piecewise functions:

$$\varepsilon_v = \varepsilon_1 + \varepsilon_2 + \varepsilon_3, \tag{1}$$

$$\varepsilon_v^{c_1} = \varepsilon_v - \frac{1 - v_{12} - v_{13}}{E_1}(\sigma_1 + \sigma_2 + \sigma_3), \tag{2}$$

$$\varepsilon_v^{c_2} = \varepsilon_v - \frac{1 - v'_{12} - v'_{13}}{E_2}(\sigma_1 + \sigma_2 + \sigma_3), \tag{3}$$

$$\varepsilon_v^{c} = \varepsilon_v^{c_1} + \varepsilon_v^{c_2}, \tag{4}$$

where ε_v is the volume strain of the specimen; ε_1, ε_2, and ε_3 are the strains in the three principal stress directions, respectively; $\varepsilon_v^{c_1}$ and $\varepsilon_v^{c_2}$ are the microcrack strain before and after the intermediate-frequency disturbance; v_{12} and v_{13} denote the Poisson's ratio v before intermediate-frequency disturbance; v'_{12} and v'_{13} are the Poisson's ratio v after intermediate-frequency disturbance; E_1 and E_2 refer to the elastic modulus before and after intermediate-frequency disturbance; ε_v^c is the total crack volume strain.

As shown in Fig. 14, σ_{cd} corresponds to the inflection point of the volumetric strain curve, where the specimen

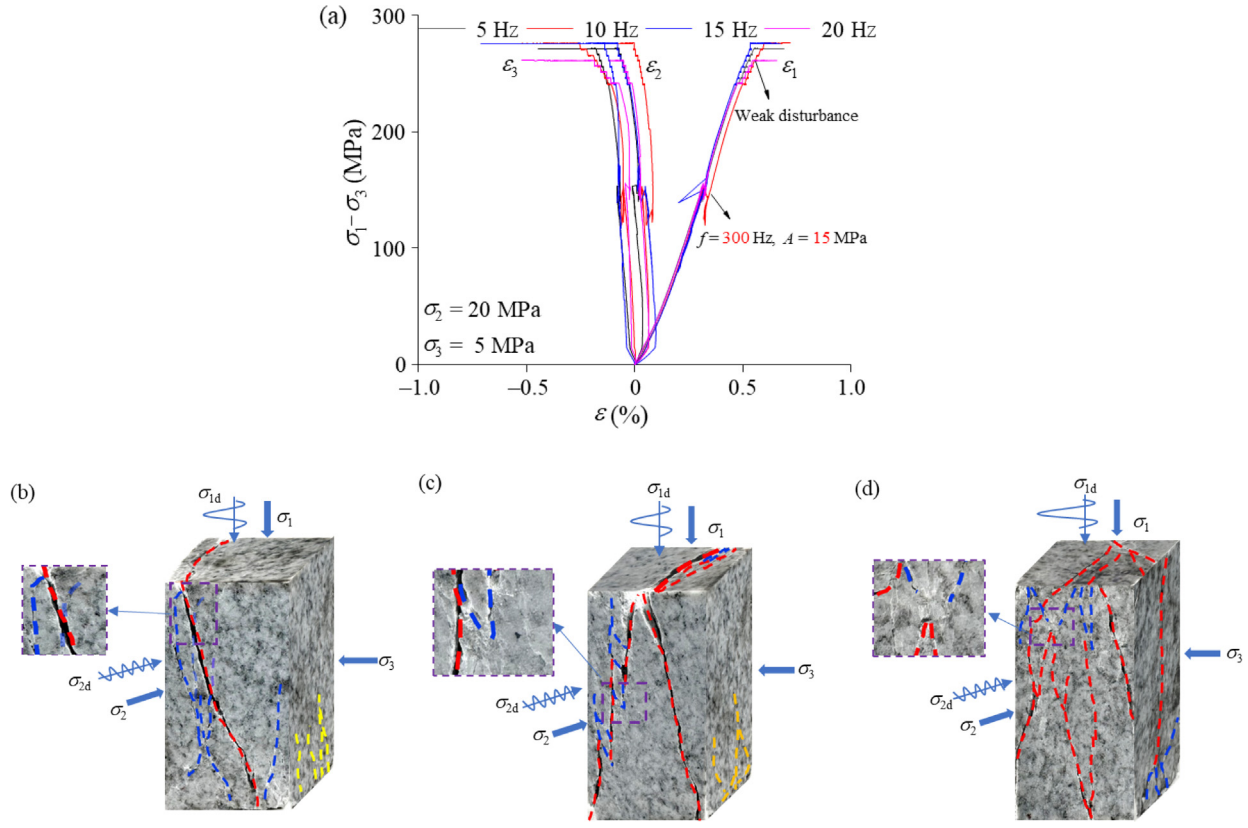

Fig. 11. Influences of different weak disturbance frequencies on the intermediate-frequency disturbance at the σ_{ci} point: (a) σ_1 comparison and the failure mode with low-frequency of (b) 5 Hz, (c) 10 Hz, and (d) 15 Hz, and Fig. 9(b) 20 Hz. There is no obvious independent tensile area in the specimen, but more tensile-shear mixed failure modes have developed.

begins to expand; σ_{ci} marks the transition of the crack volume from a vertical direction to negative values. Figure 14 (b) and (c) shows that the intermediate-frequency disturbance at σ_{ci} and σ_{cd} will change the elastic modulus E of the rock, and new values of σ'_{ci} and σ'_{cd} will appear, suggesting that the tensile cracks generated by the intermediate-frequency disturbance damage the rock mass.

Changes in the physical properties and characteristic stress under the influences of different coupled effects of intermediate and low-frequency dynamic disturbances are calculated in Table 2.

It can be observed that, for the specimens affected by intermediate-frequency disturbance at σ_{ci}, the value is increased by an average of 30%, which is approximately equal to the original σ_{cd}. Similarly, σ_{cd} of the specimens also shows an average increase of 12% due to the influence of the intermediate-frequency disturbance. Similarly, the crack volume continues to increase with the principal stress in the σ_1-direction for the specimen affected by intermediate-frequency disturbance at σ_{cd}, remaining unchanged. This results in a delay to crack initiation, indicating that the intermediate-frequency disturbance at σ_{cd} causes tensile cracks at the end of the specimen, and this is affected by the confining pressure and is completely closed at the end of the dynamic disturbance. At this time, the crack volume can make the rock generate only elastic strain under load, without generating new cracks. The new σ'_{ci} increases beyond the original value of σ_{cd} before new cracks begin to form (crack initiation). The specimen rapidly enters the damage stage once microcracks start to develop; that is, the volumetric strain causes expansion. This indicates that the intermediate-frequency disturbance at σ_{cd} changes the crack propagation process in the rock. The Poisson's ratio v of the rock is significantly decreased, indicating that the deformation of the rock specimen after intermediate-frequency disturbance in the σ_2 and σ_3-direction undergoes a short pause after the end tensile crack is generated, suggesting that the end tensile crack is ready to develop. There is a certain time delay at σ_{ci} and σ_{cd} with the specimens affected by intermediate-frequency disturbance at σ_{cc}. The primary factor contributing to the decrease in σ_p is the reduction in the elastic modulus E of the rock mass, which causes the specimen to reach its σ_p under minimal deformation.

In summary, it can be observed that the intermediate-frequency disturbance increases the elastic modulus E of the specimen, but the peak value decreases, contrary to the previous findings (Rybacki et al., 2015). The reason for this is shown in Fig. 15. The intermediate-frequency disturbance causes the specimen to undergo significant

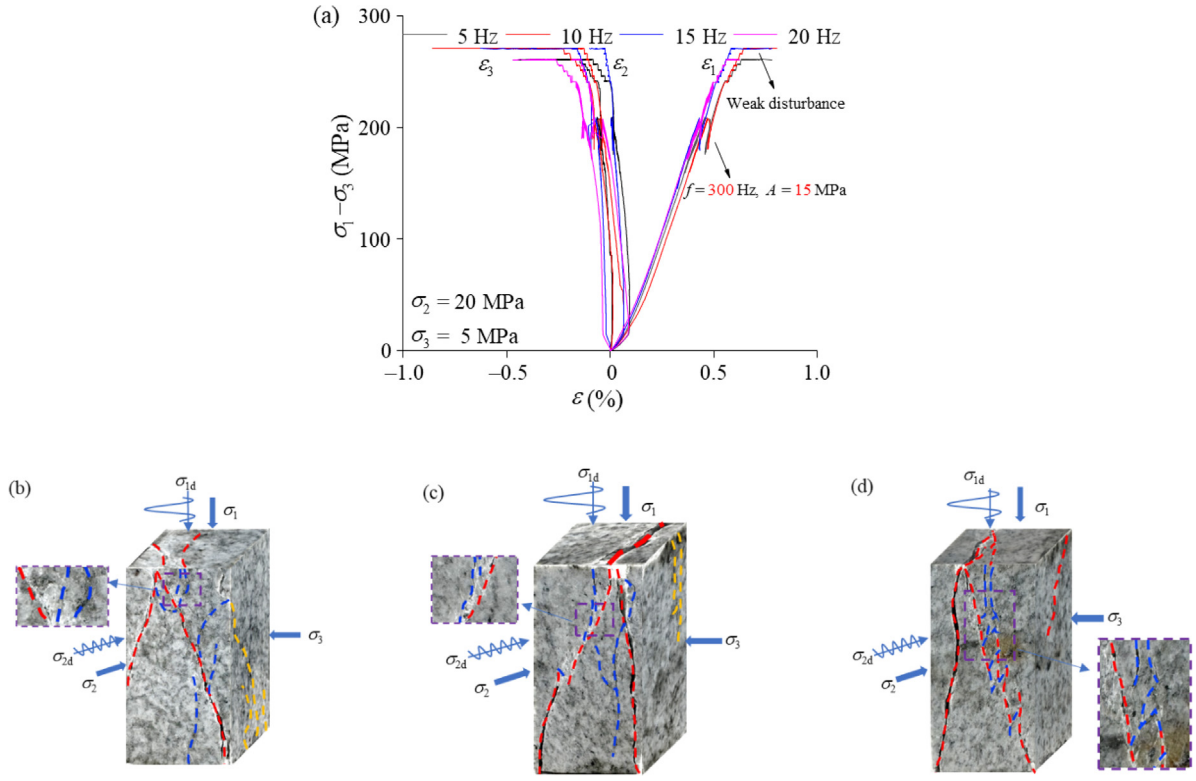

Fig. 12. Influences of different weak disturbance frequencies on the intermediate-frequency disturbance at the σ_{cd} point: (a) σ_p comparison and the failure mode with low-frequency of (b) 5 Hz, (c) 10 Hz, and (d) 15 Hz, and Fig. 9(c) 20 Hz. The crack characteristics in the tension zone become more obvious with the increase of the weak disturbance frequency.

compressive deformation immediately, leading to the generation of an elastic modulus E_2 during subsequent loading stages. This also indicates that the rock undergoes plastic deformation instantaneously due to the intermediate-frequency dynamic disturbance.

The brittleness of rock determines the tendency of crack initiation and propagation under the external stress, and σ_{ci} is the critical stress for crack initiation and propagation. Rocks with high brittleness usually have low σ_{ci}, making them more prone to crack propagation. The stress and strain statistics pertaining to rock at σ_{ci} and σ'_{ci} are summarized in Table 3, and the brittleness index B of rock is calculated using Eq. (5):

$$B = \frac{\sigma_p - \sigma_{ci}}{\sigma_p} \cdot \frac{\varepsilon_p}{\varepsilon_p - \varepsilon_{ci}}. \quad (5)$$

Among them, B_1 and B_2 represent the brittleness index of granite before and after intermediate- frequency disturbance respectively. The rock specimens induced by intermediate-frequency disturbance exhibit a significant decrease in brittleness due to the generation of new σ'_{ci}. The specimens with intermediate-frequency disturbance at σ_{cd} show a notable decrease in brittleness among them. As a result, the specimen affected by intermediate-frequency disturbance at σ_{cc} exhibits the highest brittleness and a lower peak strength.

Figure 16 depicts the effect of weak disturbance frequency on the rock brittleness index. The brittleness of the specimens affected by intermediate-frequency disturbance at σ_{cc} is the largest, and σ_p is the lowest, exerting the greatest influence on the mechanical properties. For the specimens induced by intermediate-frequency disturbance at σ_{ci} and σ_{cd}, the generation of new σ'_{ci} leads to a reduction in the brittleness of the rock during failure progress. However, the influence of the weak disturbance frequency on the brittleness index differs, being random. For the specimens subjected to intermediate-frequency disturbance at the σ_{ci} point, the brittleness index is positively correlated with σ_p of the rock. The brittleness of other specimens, which are primarily within their natural frequency ranges, significantly increases. This shows that, when considering the influence of dynamic disturbance frequency, it is necessary to consider the deleterious effect of the excitation at, or close to, the resonant frequency on the performance of the rock.

3.4 Analysis of pre-peak energy

The improved energy calculation method was adopted in this study to more accurately investigate the pre-peak energy composition of rock under the coupled effects of multiple dynamic disturbance sources (Fig. 17). Taking the σ_1-direction as a reference, the total stored energy pre-peak is partitioned into five components: the overall pre-peak stored energy of the rock denoted by S_{SOAJI}, the dis-

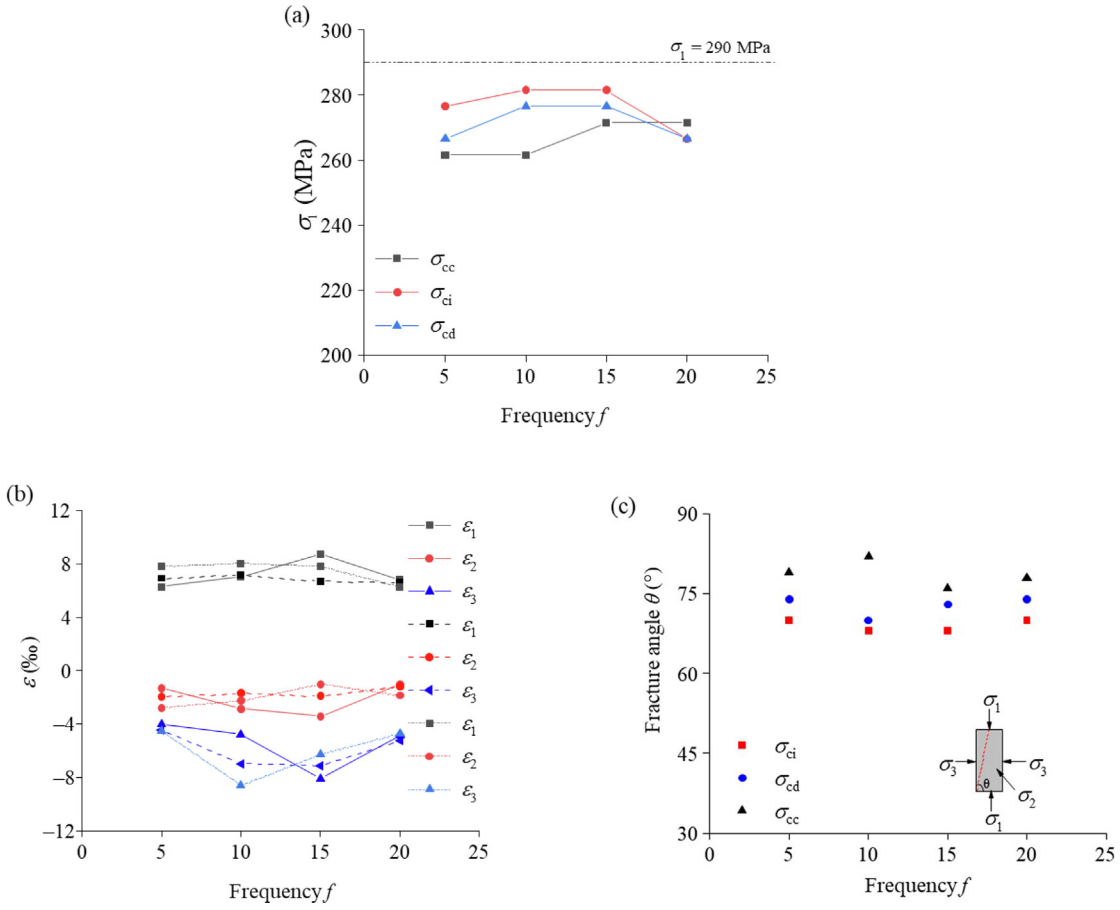

Fig. 13. Influences of intermediate-frequency disturbance time and weak disturbance frequency on the peak strength of rock. (a) σ_p comparison, (b) ε_p comparison, and (c) fracture angle.

turbance energy generated by intermediate-frequency perturbations represented by S_{FGCD}, and the disturbance energy arising from weak disturbances denoted by S_{BAJIH}. Regarding the calculation of elastic and dissipative energies mentioned herein, taking the loaded rock specimen as an example, it is assumed that the rock specimen is in the linear elastic deformation stage before the elastic limit point, and the rock only stores elastic strain energy at this stage under the external force (provided by the testing machine). Once the elastic limit is exceeded, the existing crack will expand. Driven by elastic energy, some of the stored elastic strain energy will be converted into dissipated energy along with crack propagation, while the remaining part exists in the rock specimen in the form of elastic energy. At this point, with the expansion of each existing crack or the generation of new cracks, part of the elastic strain energy required will also be dissipated, resulting in a gradual increase in total dissipative energy. From this stage onward, a portion of the stored elastic strain energy is converted into dissipative energy as existing cracks extend or new cracks form, leading to a gradual increase in energy dissipation. This shows that the mechanism of energy conversion can be fully understood from the perspective of the deformation and failure process. Therefore, the total elastic energy of rock is $S_{EAJ}+S_{OEKF}$, where the elastic energy before intermediate-frequency disturbance is S_{OALF}, and the elastic energy after intermediate-frequency disturbance is S_{KLJ}. The energy dissipated is S_{FKJIH}.

Rock energy can be calculated as follows:

$$U_{total} = U_e + U_d, \tag{6}$$

$$U_{total} = \int_0^{\varepsilon_1^t} \sigma_1 d\varepsilon_1 + \int_0^{\varepsilon_2^t} \sigma_2 d\varepsilon_2 + \int_0^{\varepsilon_3^t} \sigma_3 d\varepsilon_3, \tag{7}$$

where U_e and U_d represent the elastic energy and dissipative energy, respectively. ε_1^t, ε_2^t, and ε_3^t represent the strains in the three principal stress directions at time t.

The pre-peak energy composition of rock under the coupled effect of multiple dynamic disturbance sources is shown in Fig. 18. The elastic energy-1 represents the total pre-peak elastic energy, and the elastic energy-2 represents the elastic energy storage inside the rock after intermediate-frequency disturbance. Energy composition can be divided into the following two influencing factors:

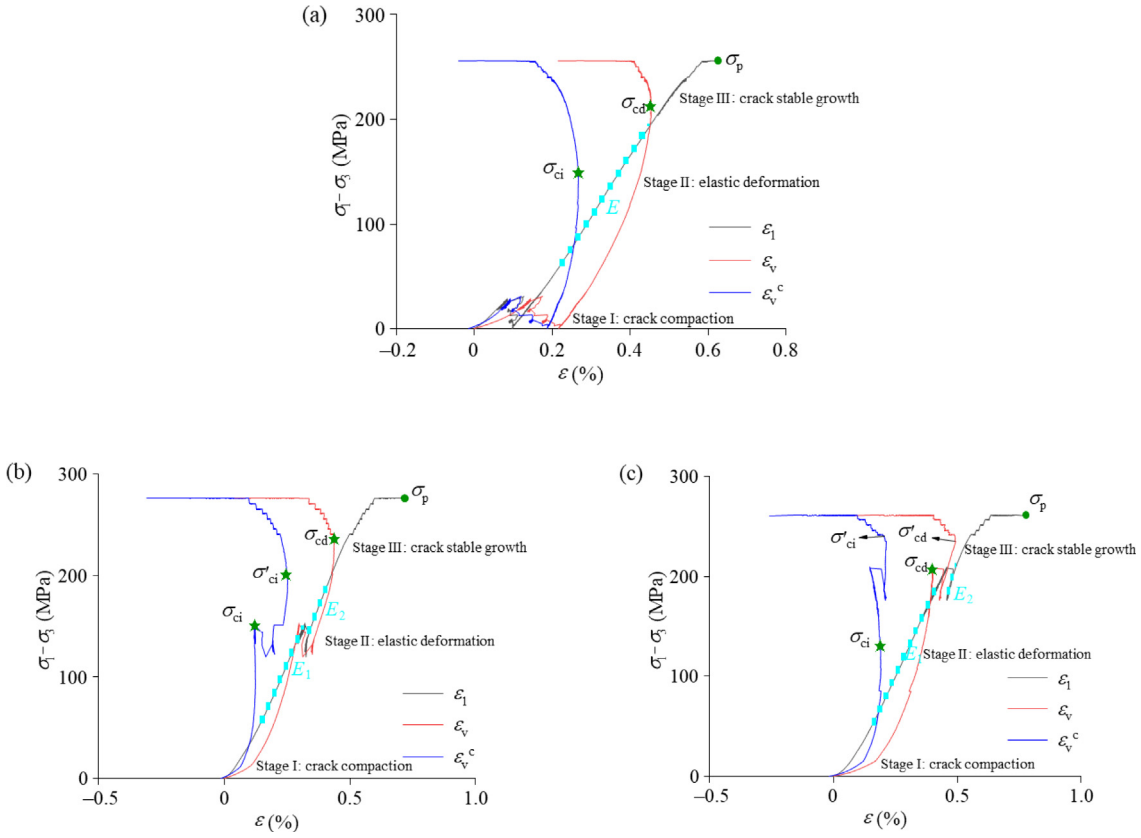

Fig. 14. Typical characteristic stress curves and the intermediate-frequency dynamic disturbance point at (a) σ_{cc}, (b) σ_{ci}, and (c) σ_{cd}.

Table 2
Characteristic stress and physical properties of granite under intermediate-frequency disturbance.

Disturbance timing	f (Hz)	σ_{ci} (MPa)	σ'_{ci} (MPa)	σ_{cd} (MPa)	σ'_{cd} (MPa)	v	v'	E_1 (GPa)	E_2 (GPa)	σ_p (MPa)
Intermediate-frequency disturbance at σ_{ci}	5	157	203	239	–	0.221	0.318	56.4	73.6	276.5
	10	157	191	214	241	0.224	0.170	53.9	71.6	281.5
	15	157	210	241	–	0.231	0.149	59.0	68.1	281.5
	20	157	202	238	–	0.210	0.132	56.5	79.0	266.5
Intermediate-frequency disturbance at σ_{cd}	5	164	240	214	243	0.23	0.05	57.0	78.7	266.5
	10	111	219	214	235	0.30	0.05	49.5	67.0	276.5
	15	170	234	214	245	0.21	0.05	58.0	69.4	276.5
	20	148	229	210	236	0.34	0.37	55.7	63.9	266.5
Intermediate-frequency disturbance at σ_{cc}	5	159	–	217	–	0.23	–	60.8	–	261.5
	10	149	–	236	–	0.21	–	61.8	–	261.5
	15	144	–	226	–	0.26	–	60.4	–	271.5
	20	118	–	217	–	0.22	–	58.3	–	271.5

(1) Influence of intermediate-frequency disturbance

The energy generated by intermediate-frequency disturbance (pink line) is $\sigma_{cd} > \sigma_{ci} > \sigma_{cc}$, and the energy generated by intermediate-frequency disturbance at σ_{cc} is the most stable. On the contrary, the energy randomness generated by the intermediate-frequency disturbance at σ_{cd} is the largest. The elastic energy after intermediate-frequency perturbation also shows this phenomenon, which indicates that σ_{cd} represents the most unstable crack development stage in different intermediate-frequency perturbation timings, leading to a large dispersion of the energy distribution. The total energy (green line): $\sigma_{cd} > \sigma_{ci} > \sigma_{cc}$, combined with the peak comparison, indicates that the intermediate-frequency disturbance at the σ_{cd} point has the highest degree of rock performance cracking, so that it has higher pre-peak energy storage and lower peak strength. These two points are the key factors indicating the onset of a rockburst.

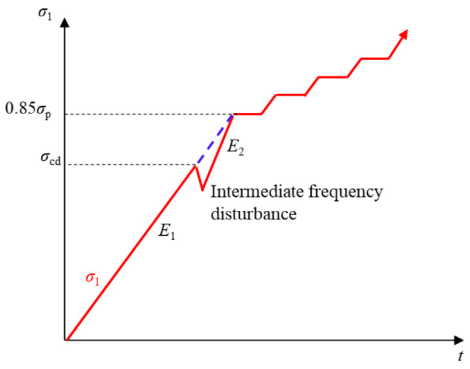

Fig. 15. Increase of the rock elastic modulus E as a result of intermediate-frequency disturbance.

(2) Influences of intermediate and low-frequency disturbance

The pre-peak elastic energy (red line) of rock subjected to the coupled effects of intermediate and low-frequency dynamic disturbances is $\sigma_{ci} > \sigma_{cd} > \sigma_{cc}$. This indicated that the more obvious the intermediate-frequency disturbance effect, the more independent tensile cracks generated at the end, and the weaker the pre-peak elastic energy storage capacity of the rock. The pre-peak energy storage is still strongly correlated with the natural frequency of the rock due to the influence of the weak disturbance frequency. An interesting phenomenon arises here: when the resonance effect occurs, the storage capacity of the pre-peak elastic energy of the rock will be significantly reduced. This elastic energy will be converted into dissipated energy (black line), and the increase in dissipated energy represents the expansion of internal microcracks or the generation of new cracks, which indicates the promotional effect of resonance on rock failure.

3.5 Influences of weak disturbance amplitude and directions

Figure 19 demonstrates the stress–strain curves and failure modes of granite subjected to different weak disturbance amplitudes after intermediate-frequency disturbance at σ_{ci}. By selecting a dynamic disturbance frequency of 20 Hz and amplitudes of = 1, 3, and 5 MPa, the σ_p of the rock are 266.5, 261.5, and 261.5 MPa, respectively. The results show that the peak strength of rock still decreases with the increase of dynamic disturbance amplitude A, but the decrease is not obvious. Only the peak strain at $A = 5$ MPa is significantly higher than that at 1 MPa, and the peak strength does not change to any significant extent. This shows that the factors influencing the dynamic disturbance amplitude A should include the ratio of disturbance amplitude to the original static stress, that is A/σ. The influence of unloading stress on rock failure warrants attention when evaluating the effects of any such dynamic disturbance. In the present study, $A/\sigma_2 = 0.05$, 0.15, and 0.25, and it is evident that the unloading effect is negligible. In contrast, the differences in failure modes induced by disturbance amplitudes A are more significant. It can be observed that the macroscopic crack morphology transitions from shear-dominated to tensile failure, with through-shear cracks appearing in the σ_3-direction under the influence of resonance. The increase of weak disturbance amplitude increases the range of influence of tensile cracking at the end of the specimen.

The stress–strain curves and failure modes of granite under different weak disturbance directions (σ_2- and σ_3-direction) after intermediate-frequency disturbance at σ_{cd} are presented in Fig. 20. The σ_p of the rock is 266.5 MPa under σ_2-direction disturbance and 261.5 MPa under σ_3-direction disturbance at $f = 20$ Hz (within the natural frequency range) and A = 1 MPa. The difference persists in the failure modes. Dynamic disturbance applied in the σ_3-direction promotes more tensile cracking, which induces a greater volumetric strain when brittle failure occurs. To conclude, the influence of the dynamic disturbance direction on the σ_p of the rock is essentially attributed to the unloading stress effect during the dynamic disturbance process as mentioned. For this study, when dynamic disturbance is applied in the σ_2-direction, $A/\sigma_2 = 0.05$; when applied in the σ_3-direction, $A/\sigma_3 = 0.2$. The unloading effect is negligible in both cases, which is the reason for the negligible difference in peak strength.

Table 3
Brittleness index of granite under different intermediate-frequency disturbance timings.

Timing of dynamic disturbance application	f (Hz)	ε_{ci} (%)	ε'_{ci} (%)	ε_p (%)	B_1	B_2
Intermediate-frequency disturbance at σ_{ci}	5	0.319 43	0.419 15	0.717 93	0.78	0.64
	10	0.318 00	0.399 55	0.700 27	0.78	0.75
	15	0.359 03	0.473 53	0.747 50	0.85	0.69
	20	0.312 21	0.387 87	0.658 78	0.78	0.59
Intermediate-frequency disturbance at σ_{cd}	5	0.341 57	0.500 56	0.780 71	0.68	0.28
	10	0.283 10	0.508 24	0.803 02	0.92	0.57
	15	0.351 53	0.490 66	0.780 71	0.70	0.41
	20	0.310 86	0.464 81	0.625 95	0.88	0.55
Intermediate-frequency disturbance at σ_{cc}	5	0.378 76	–	0.627 11	0.98	–
	10	0.383 68	–	0.701 88	0.95	–
	15	0.360 02	–	0.615 16	0.88	–
	20	0.280 96	–	0.680 20	0.96	–

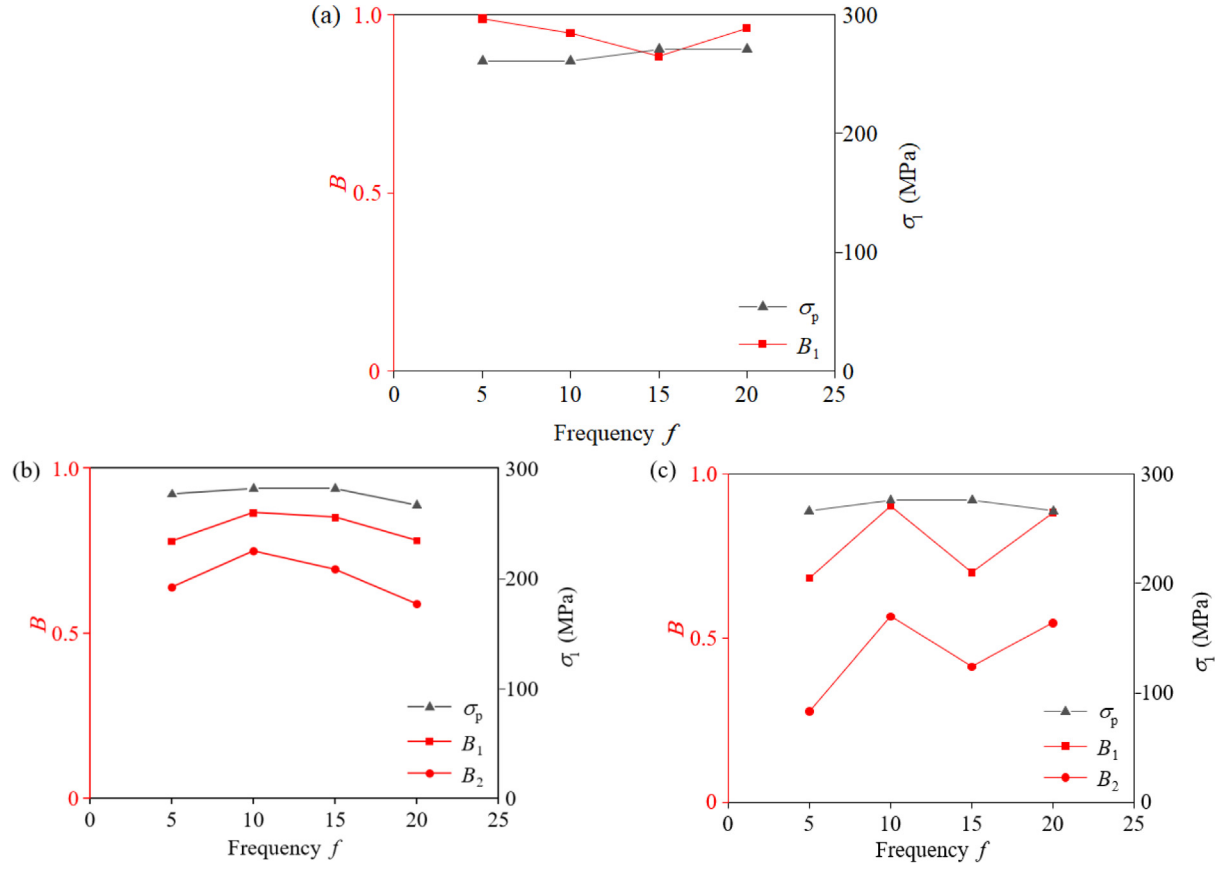

Fig. 16. Rock brittleness index B before and after intermediate-frequency disturbance with the intermediate-frequency disturbance points of (a) σ_{cc}, (b) σ_{ci}, and (c) σ_{cd}.

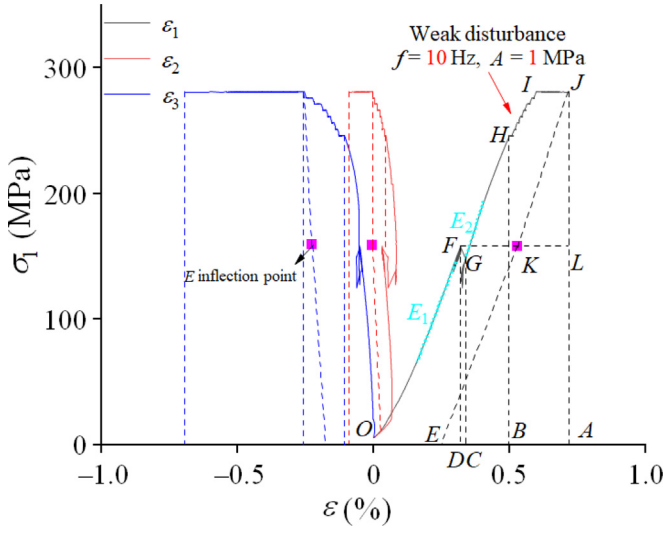

Fig. 17. Calculation of pre-peak energy of granite. It is worth noting that the line JE is not a straight line, but represents the change of rock elastic modulus E caused by the intermediate-frequency disturbance. The point K represents the point of inflection of the elastic modulus E.

4 Discussion

4.1 Mechanism of rock failure under the coupled effects of intermediate and low-frequency disturbances

Failure of the rock under the coupled effects of intermediate and low-frequency events exhibits distinct spatial–temporal characteristics, thus forming a more complex tension-shear mixed failure mode. The intermediate-frequency disturbance is always applied before the low-frequency disturbance in this study, and the mechanism underpinning tensile-shear mixed failure of rock under the coupled effects of intermediate and low-frequencies is shown in Fig. 21. The intermediate-frequency disturbance (f = 300 Hz) acts on the tangential direction of the tunnel (corresponding to the σ_1-direction), resulting in tensile microcracks, but the cracks only exist near the end and do not form penetration. Then, the stress concentration occurs in the σ_1-direction. The rock is affected by the weak disturbance frequency under different working conditions of f = 0–20 Hz in the axial direction of the tunnel (corresponding to the σ_2-direction), which promotes the

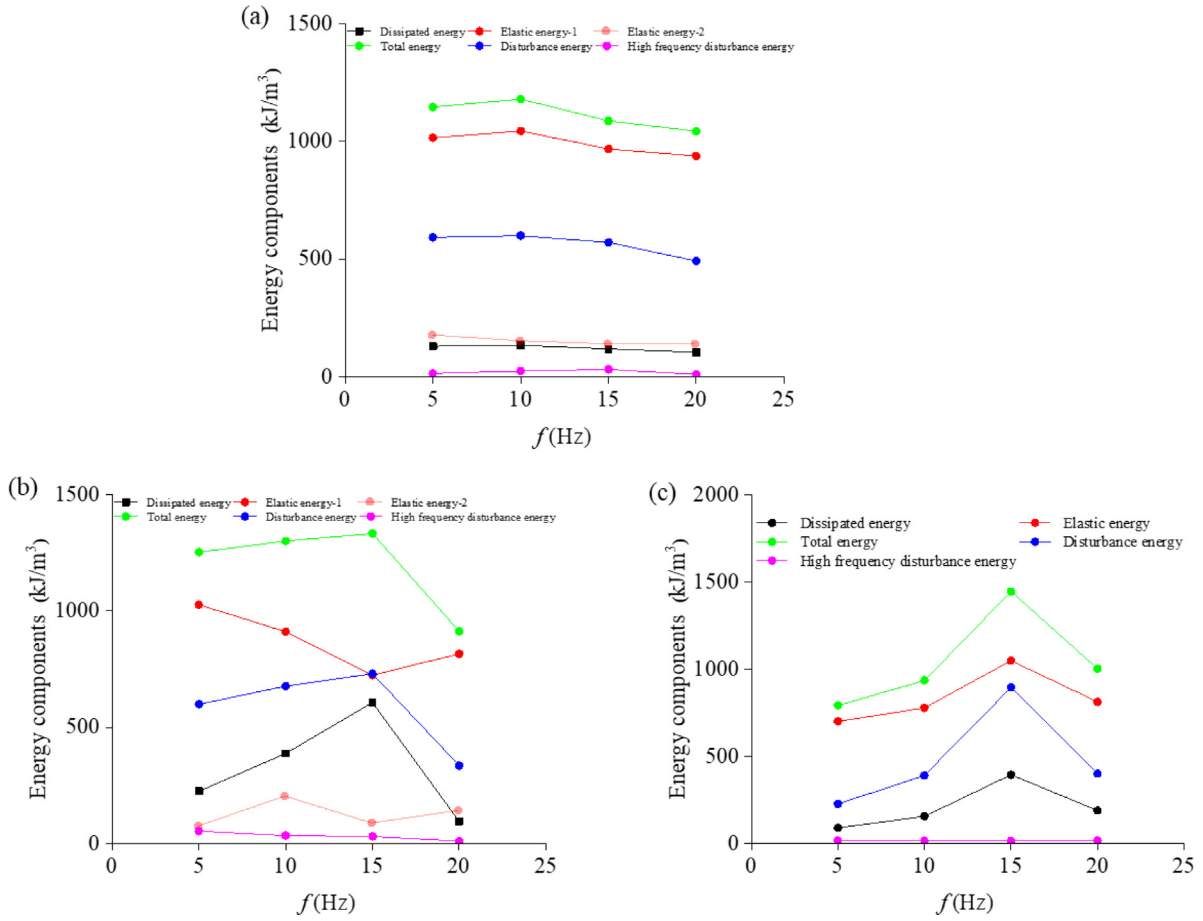

Fig. 18. Typical characteristic stress curves and the intermediate-frequency dynamic disturbance point at (a) σ_{ci}, (b) σ_{cd}, and (c) σ_{cc}.

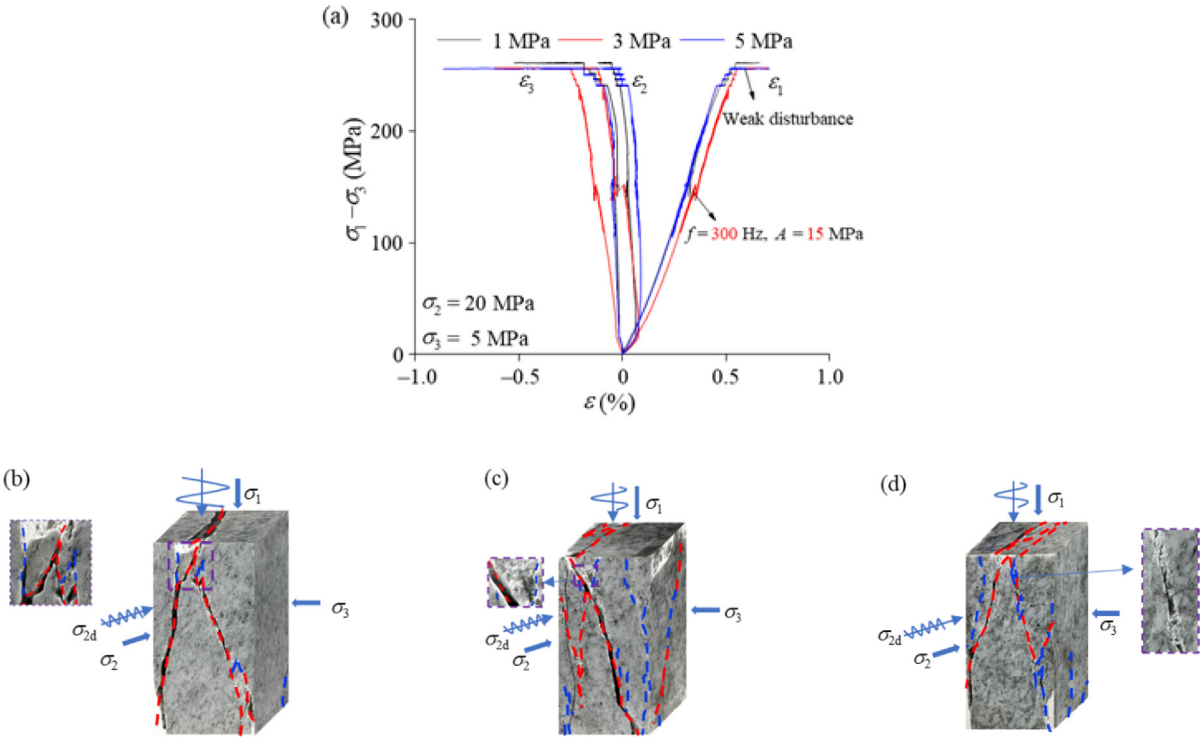

Fig. 19. Peak strength of rock brittle failure under the influences of different weak disturbance amplitudes at the intermediate-frequency disturbance timing. (a) σ_1 comparison, failure mode of (b) $A = 1$ MPa, (c) $A = 3$ MPa, and (d) $A = 5$ MPa.

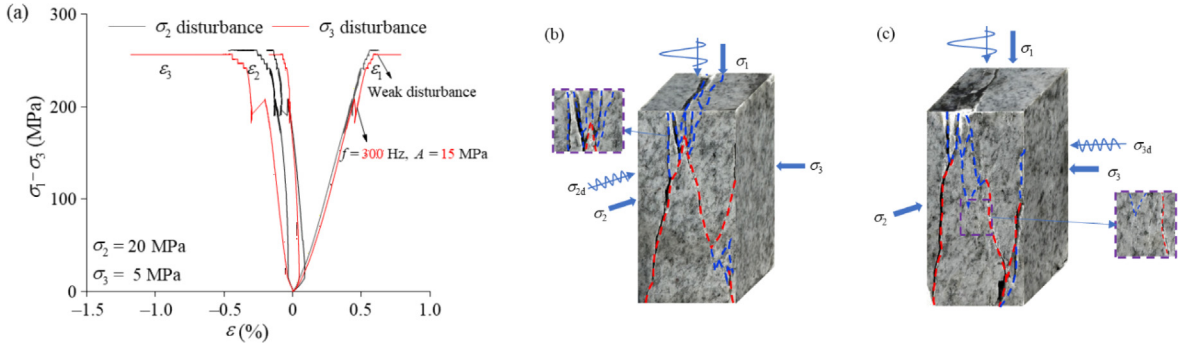

Fig. 20. Peak strength of rock under the influence of different weak disturbance directions at the same intermediate-frequency disturbance time. (a) σ_1 comparison. Failure mode: (b) weak disturbance in the σ_2-direction, and (c) weak disturbance in the σ_3-direction.

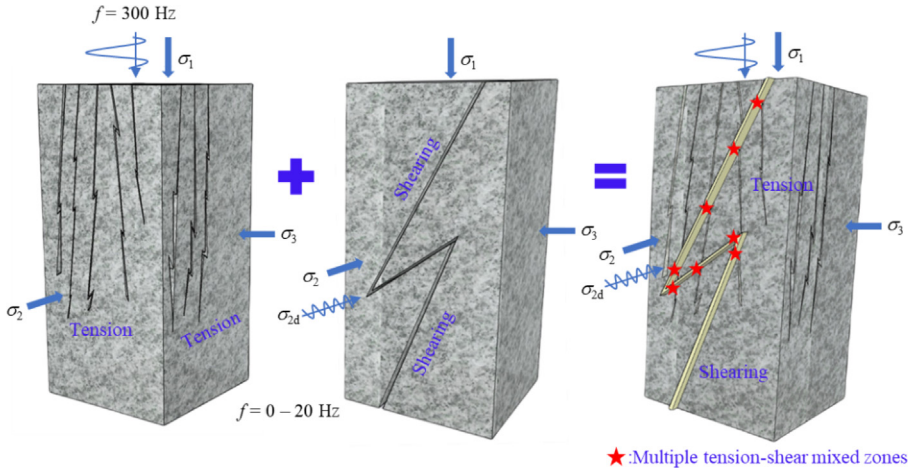

Fig. 21. Formation of the tensile-shear mixed fracture mode of specimens.

formation of shearing cracks. Affected by this, the σ_1-direction is further concentrated, and the pre-damaged rock (intermediate-frequency disturbance produces tensile cracks) is under the influence of high static, cumulative, multiple, as well as long-term dynamic disturbances. Finally, brittle fracture occurs, forming multiple, independent, and mixed-fracture areas.

Previous studies on the failure mode of rock under true triaxial stress conditions showed that the failure surface always appears on the intermediate principal stress (σ_2) surface, extending to the minimum principal stress surface (σ_3), and finally forming a breakthrough after which brittle failure occurs (Feng et al., 2019). This suggests that the length of tensile cracks in the σ_3-direction surface is unrelated to the peak strength of the rock, but is affected by the resonance effect and the timing of intermediate-frequency disturbance. The earlier the initiation of end-face tensile cracks during the rock loading phase, the greater the probability of these cracks appearing on the σ_3-direction surface, thereby increasing the probability of forming through-cracks.

4.2 Resonance effects induced by weak disturbances

When the frequency of dynamic disturbances aligns with the natural frequency of the rock under specific stress conditions, resonance may develop. The energy amplification effect occurs when the external dynamic disturbance frequency approaches or equals the natural frequency of the rock, leading to a significant increase in the vibration amplitude of the rock. The natural frequency of the rock is related to its density ρ, elastic modulus E, geometric characteristics, etc. The resonance effect generated under these conditions can lead to stress concentration within the rock, promoting the development of microcracks, decreasing peak strength, and facilitating brittle failure of the rock (Johnson et al., 1996). This study used the time-strain curve of the rock during first-stage loading under the influences of different weak disturbance frequencies as an example to verify this interesting phenomenon (Fig. 22). For specimens subjected to intermediate-frequency disturbance at σ_{cd} and σ_{ci}, significant vibrations in the amplitude of rock strain occur at frequencies

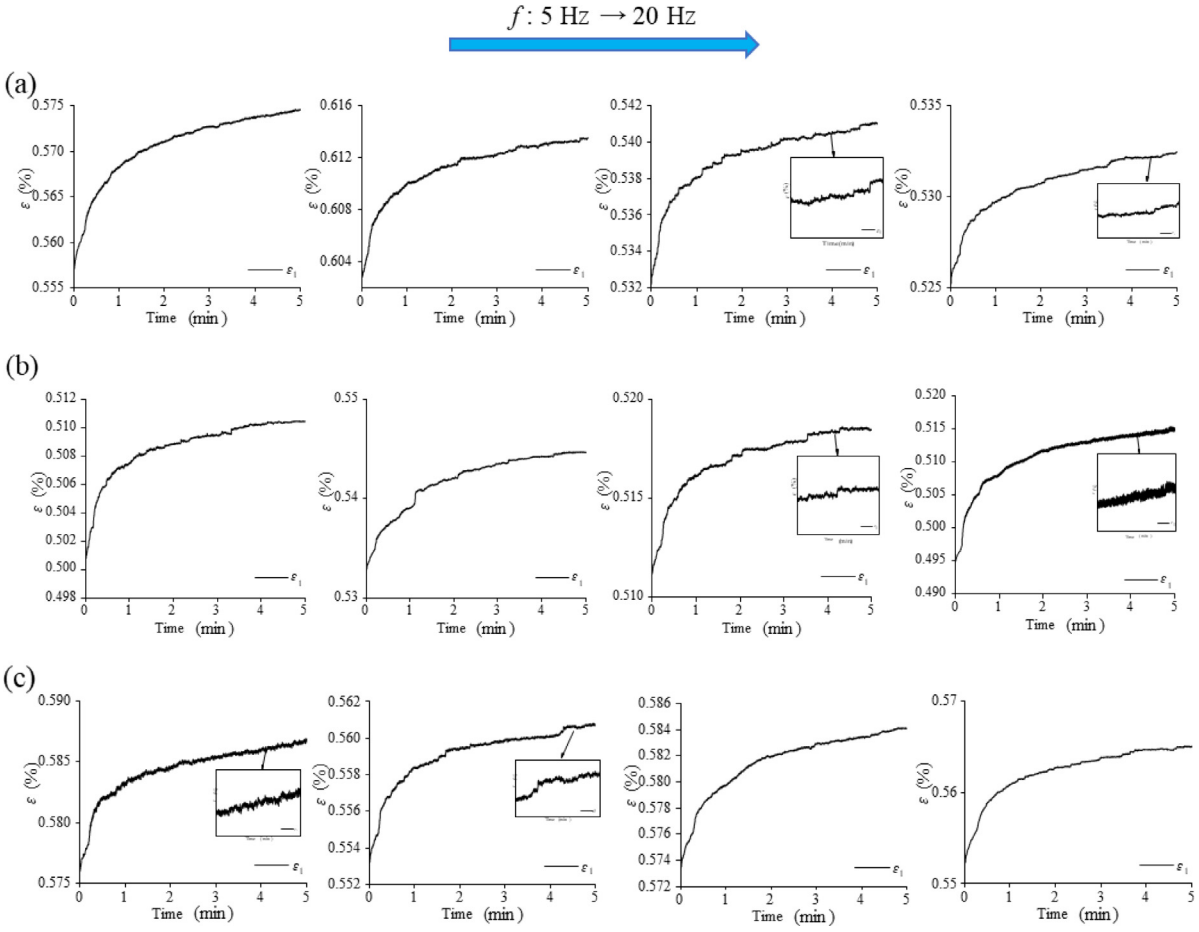

Fig. 22. Time-strain curves of rock under dynamic disturbance and the intermediate-frequency dynamic disturbance are applied at (a) σ_{cd}, (b) σ_{ci}, and (c) σ_{cc}.

between 15 and 20 Hz during the first-stage weak disturbance loading process. The curve shape indicates that the rock specimen may have undergone a certain degree of resonance effect at this dynamic disturbance frequency. This is particularly evident in the specimen subjected to intermediate-frequency disturbance at σ_{ci} with a frequency of 20 Hz. For specimens subjected to intermediate-frequency disturbance at σ_{cc}, a greater number of tensile cracks are generated internally. The crack volume reaches its maximum, resulting in lower stiffness compared to other specimens as the principal stress increases. This reduction in stiffness lowers the natural frequency of the rock, causing resonance effects to occur at frequencies between 5 and 10 Hz.

4.3 Analysis of macro and microscopic failure surface

Three rock specimens subjected to different intermediate-frequency disturbance timings were selected for failure surface scanning, and the scanned images are shown in Fig. 23. The joint roughness coefficient (JRC) in region a of the figure is significantly higher than that in region b, indicating that region a represents rough tensile cracks, while region b corresponds to smooth shearing cracks (Barton et al., 2023). The overlapping area between regions a and b represents the independent tensile-shear mixed failure zones formed under the coupled effects of low and intermediate-frequency dynamic disturbances. It can be concluded that tensile cracks precede shearing cracks during the crack initiation process in the rock by examining the failure surface. The specific process can be described as follows:

(1) From onset of loading to intermediate-frequency disturbance

The specimens undergo pore compression and solid particle compression stages, the subsequent rocks undergo intermediate-frequency disturbance in the crack initiation stage or crack damage stage, and the tensile crack is generated at the end of the specimens. Currently, there is no obvious shear crack within.

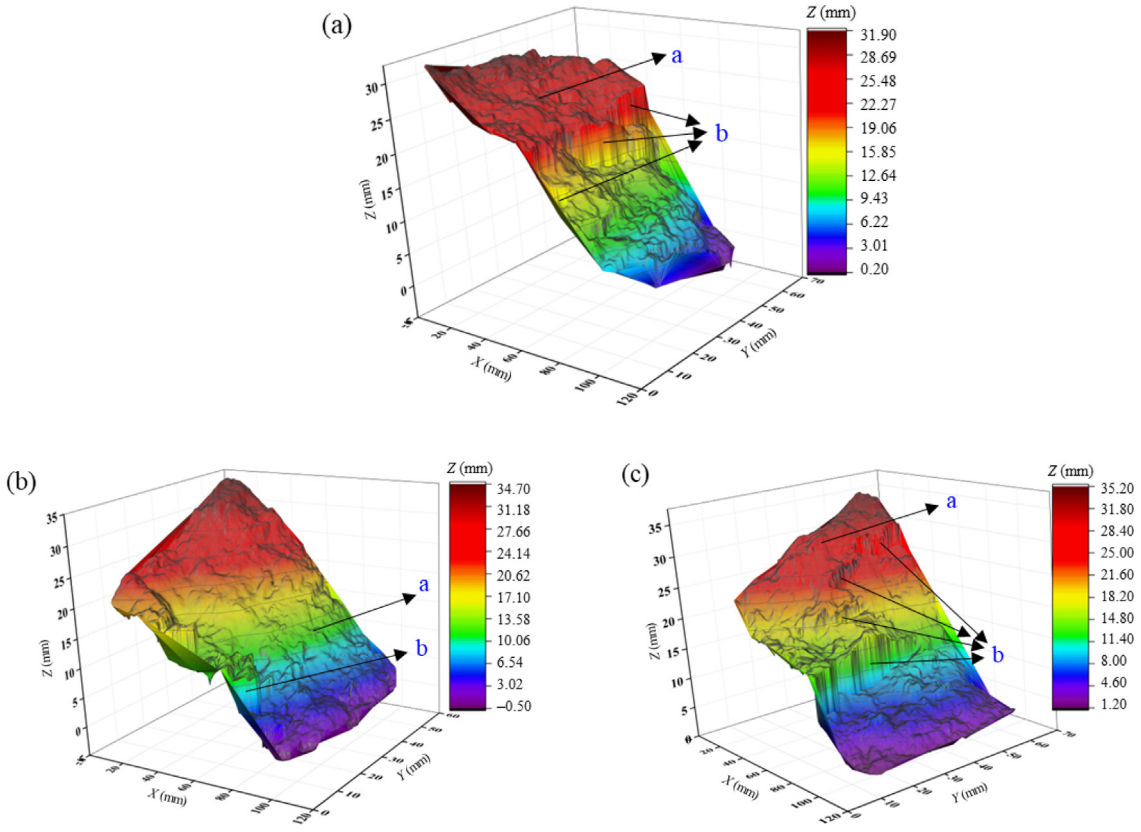

Fig. 23. Scanning of granite fracture surface at different intermediate-frequency disturbance timings. (a) σ_{cc}, (b) σ_{ci}, and (c) σ_{cd}.

(2) From intermediate-frequency disturbance to weak disturbance

Tensile cracks gradually develop as the principal stress increases. The cracks exhibit a pulling pattern with noticeable rotation under the condition of increasing principal stress. Shear cracks may appear within a small localised region.

(3) From weak disturbance to σ_p

Tensile cracks develop rapidly under the influence of repeated dynamic disturbance loading in the σ_2-direction. As the deviator stress (σ_1–σ_3) increases, the small tensile cracks in different rock layers coalesce, forming through-cracks and leading to the appearance of smooth shearing cracks, as shown in region b in Fig. 23. At this stage, the microcracks in the specimen develop and propagate, forming a macroscopic failure surface. The rock reaches its peak strength, and the specimen becomes instantaneously unstable, resulting in brittle failure.

The failure surface described above was scanned using a scanning electron microscope (Fig. 24). There is a small range of tensile-shear cracks caused by low-frequency disturbance (Fig. 24(a)). Distinct shear tearing ridges and tensile twisting phenomena are clearly visible. The cracks bypass the crystalline particles in the rock, forming intergranular fractures, which symbolise the initial development of cracks. Figure 24(b) shows the smooth cracks and debris generated by intermediate-frequency disturbance, primarily located near the end of the specimen. The cross-section appears as a layered stacking of fragments. Figure 24(c) shows distinct shear tearing ridges, corresponding to region b (Fig. 23). The shear cracks in this area are relatively independent, with a clear ridge-like displacement structure. The crack propagation clearly intersects the solid particles in the rock. This indicates that, upon crack formation, the solid particles in the rock have already lost their load-bearing capacity in the crack region, and brittle failure occurs immediately upon crack propagation. In Fig. 24(d), the crack corresponds to the intersection of the regions a and b in Fig. 23. This area represents a distinct tensile-shear mixed fracture zone, where the crack traverses the grain interior, exhibiting a complex morphology, accompanied by a tearing area. The crack propagation direction is irregularly induced by the coupled effects of dynamic disturbance, the arrangement of grain particles, and the internal structure of the material, reflecting the characteristics of brittle failure.

5 Conclusions

(1) The coupled effects of intermediate and low-frequency dynamic disturbances significantly affect the σ_p and ε_p of rock. The σ_p of the rock decreases

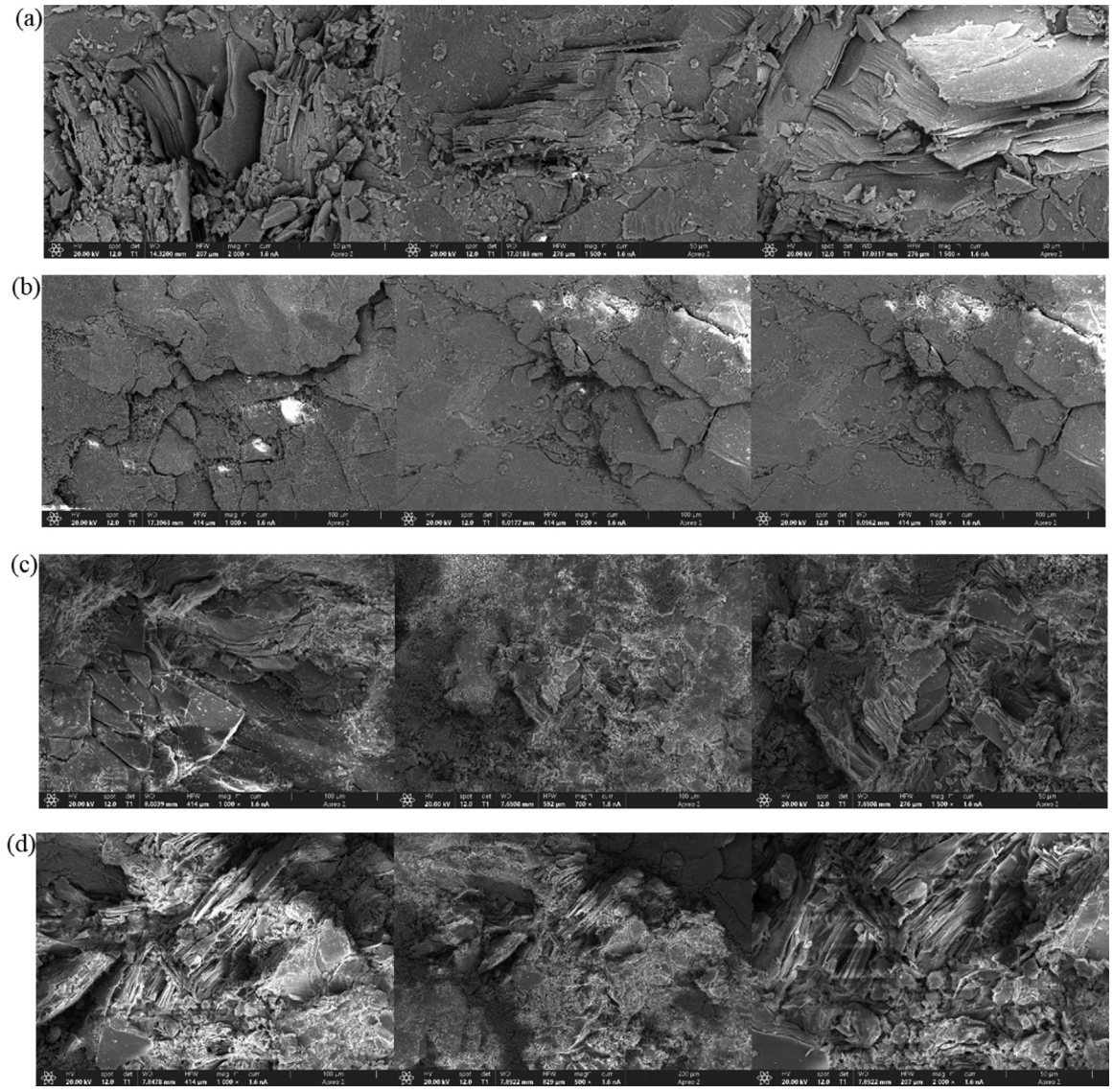

Fig. 24. Scanning electron microscope imaging. (a) Micro-shear and tensile cracks of rock under weak disturbance loading, (b) rock debris produced by intermediate-frequency disturbance, (c) shearing crack region, and (d) complicated tension-shear region.

by 8.1% to 9.8% under the combined influence of intermediate-frequency dynamic disturbance ($f = 300$ Hz) and low-frequency dynamic disturbance ($f = 5$–20 Hz) compared to the undisturbed rock. Notably, the largest decrease in the peak strength occurs when an intermediate-frequency disturbance is applied during the σ_{cc} stage. Furthermore, as the low-frequency disturbance frequency increases from 5 to 20 Hz, the σ_p of the rock follows a U-shaped trend, with a decreasing amplitude of 15 MPa.

(2) Intermediate and low-frequency dynamic disturbances significantly alter the characteristic stress on the rock, including the crack initiation stress (σ_{ci}) and the damage stress (σ_{cd}). The intermediate-frequency disturbance induces the early initiation of cracks, leading to an increase in σ'_{ci} from 157 to 234 MPa (an increase of 49%) and in σ'_{cd} from 214 to 245 MPa (an increase of 14.5%). At the same time, the elastic modulus E of the rock increases from 57.7 to 73.6 GPa (an increase of 27.6%). Intermediate-frequency disturbance of σ_{ci} and σ_{cd} significantly reduces the brittleness index of the rock and enhances the resistance to crack initiation.

(3) An energy calculation method considering the effects of intermediate and low-frequency dynamic disturbances was proposed to elucidate the pre-peak energy. The energy differences induced by intermediate-frequency disturbances at different characteristic stress points are significant, with the total pre-peak energy as follows: $\sigma_{cd} > \sigma_{ci} > \sigma_{cc}$. The energy induced by low-frequency disturbance is greatly influenced by the matching of disturbance frequency with the natural frequency of the rock. Reso-

nance effects lead to an increase in the energy associated with the imposed disturbance and a significant decrease in σ_p when the frequency approaches the natural frequency of the rock. Additionally, the pre-damage effect of intermediate-frequency disturbances further affects the sensitivity of the rock to low-frequency disturbances. The ability of the rock to store elastic energy before mobilising its peak strength is significantly reduced, with more energy being dissipated. This intensifies crack propagation and initiation, ultimately accelerating the brittle failure of the rock.

(4) The coupled effects of dynamic disturbances induce a tensile-shear mixed failure mode in the rock. Intermediate-frequency disturbances lead to the initiation and propagation of cracks along the σ_1-direction, while low-frequency disturbances further promote the development of through-going cracks in the σ_3-direction. Fracture surface analysis shows that the distribution of internal cracks in the rock exhibits higher connectivity and complexity. The tensile cracks are connected by shear cracks, and brittle failure occurs.

The experiment reveals the significant coupling between the dynamic disturbance response of the rock and its natural frequency. Different intermediate-frequency disturbances can affect the morphology of the tensile cracks in the rock, which in turn alters the stiffness of the rock specimen and ultimately changes its natural frequency. When the frequency of the low-frequency dynamic disturbance is close to the natural frequency of the rock, the rock has a significant resonance effect, and the σ_p of the rock follows a U-shaped trend. In addition, the effect of natural frequency accelerates crack propagation at specific frequencies, which leads to earlier onset of failure and greater volumetric strain. This phenomenon provides a theoretical basis for the assessment of the mechanical behaviour of the rock surrounding deep-buried tunnels under complex dynamic disturbance conditions.

Data availability

The data that support the findings of this study are available from the corresponding author upon reasonable request.

CRediT authorship contribution statement

Han-Yi Liu: Writing – original draft, Methodology, Investigation, Formal analysis, Data curation. **Ben-Guo He:** Writing – review & editing, Supervision, Resources, Project administration, Funding acquisition, Conceptualization. **Jia-Hua Guan:** Validation, Software. **Hong-Yuan Fu:** Visualization.

Declaration of competing interest

The authors declare that they have no known competing financial interests or personal relationships that could have appeared to influence the work reported in this paper.

Acknowledgement

This work was supported by the National Key R&D Program of China (Grant No. 2023YFB2603602) and the National Natural Science Foundation of China (Grant Nos. 52222810 and 52178383).

References

AyalaCarcedo, F. (2017). Drilling and blasting of rocks. Routledge.
Bahrani, N., & Kaiser, P. K. (2017). Estimation of confined peak strength of crack-damaged rocks. *Rock Mechanics and Rock Engineering, 50*(2), 309–326.
Barton, N. (2012). Reducing risk in long deep tunnels by using TBM and drill-and-blast methods in the same project - the hybrid solution. *Journal of Rock Mechanics and Geotechnical Engineering, 4*(2), 115–126.
Barton, N., Wang, C. S., & Yong, R. (2023). Advances in joint roughness coefficient (JRC) and its engineering applications. *Journal of Rock Mechanics and Geotechnical Engineering, 15*(12), 3352–3379.
Dai, F., Zhu, W. C., Ren, M., Niu, L. L., & Hou, C. (2023). Experimental and numerical simulation on the sliding process of roof rock blocks triggered by dynamic disturbance. *Underground Space, 10*, 269–293.
Eberhardt, E., Stead, D., & Stimpson, B. (1999). Effects of sample disturbance on the stress-induced micro-fracturing characteristics of brittle rock. *Canadian Geotechnical Journal, 36*(2), 239–250.
Falls, S. D., & Young, R. P. (1998). Acoustic emission and ultrasonic-velocity methods used to characterise the excavation disturbance associated with deep tunnels in hard rock. *Tectonophysics, 289*(1/2/3), 1–15.
Feng, X. T., Xiao, Y. S., & Feng, G. L. (2012). Mechanism, warning and dynamic control of rockburst evolution process. *ISRM Regional Symposium - 7th Asian Rock Mechanics Symposium.* .
Feng, X. T., Kong, R., Zhang, X., & Yang, C. (2019). Experimental study of failure differences in hard rock under true triaxial compression. *Rock Mechanics and Rock Engineering, 52*(7), 2109–2122.
Feng, X. T., Tian, M., Yang, C. X., & He, B. G. (2023). A testing system to understand rock fracturing processes induced by different dynamic disturbances under true triaxial compression. *Journal of Rock Mechanics and Geotechnical Engineering, 15*(1), 102–118.
Haimson, B. (2006). True triaxial stresses and the brittle fracture of rock. *Pure and Applied Geophysics, 163*(5), 1101–1130.
He, B. G., Wang, L., Feng, X. T., & Zhen, R. L. (2023). Failure modes of jointed granite subjected to weak dynamic disturbance under true-triaxial compression. *Rock Mechanics and Rock Engineering, 56*(11), 7939–7957.
Ingraffea, A. R. (1987). Theory of crack initiation and propagation in rock. *Fracture mechanics of rock, 10*, 71–110.
Jiang, J. Q., Su, G. S., Liu, Y. X., Zhao, G. F., & Yan, X. Y. (2021). Effect of the propagation direction of the weak dynamic disturbance on rock failure: An experimental study. *Bulletin of Engineering Geology and the Environment, 80*(2), 1507–1521.
Johnson, P. A., Zinszner, B., & Rasolofosaon, P. N. (1996). Resonance and elastic nonlinear phenomena in rock. *Journal of Geophysical Research: Solid Earth, 101*(B5), 11553–11564.
Lamert, A., Nguyen, L. T., Friederich, W., & Nestorović, T. (2018). Imaging disturbance zones ahead of a tunnel by elastic full-waveform inversion: Adjoint gradient based inversion vs. parameter space reduction using a level-set method. *Underground Space, 3*(1), 21–33.
Li, X. B., Li, C., Cao, W., & Tao, M. (2018). Dynamic stress concentration and energy evolution of deep-buried tunnels under blasting loads. *International Journal of Rock Mechanics and Mining Sciences, 104*, 131–146.

Li, X. B., Cao, W. Z., Zhou, Z. L., & Zou, Y. (2014). Influence of stress path on excavation unloading response. *Tunnelling and Underground Space Technology, 42*, 237–246.

Liu, M. B., Liao, S. M., Men, Y. Q., Xing, H. T., Liu, H., & Sun, L. Y. (2022). Field monitoring of TBM vibration during excavating changing stratum: Patterns and ground identification. *Rock Mechanics and Rock Engineering, 55*(3), 1481–1498.

Luo, H., Tao, M., Hong, Z. X., Xiang, G. L., & Wu, C. Q. (2025). Analysis of the dynamic response and damage characteristic for the tunnel under near-field blasts and far-field earthquakes. *Underground Space, 21*, 331–351.

Majedi, M., Afrazi, M., & Fakhimi, A. (2020). FEM-BPM simulation of SHPB testing for measurement of rock tensile strength. In *ARMA US Rock Mechanics/Geomechanics Symposium* (pp. 1434). ARMA.

Mishra, S., Chakraborty, T., & Matsagar, V. (2017). Dynamic characterization of himalayan quartzite using SHPB. *Procedia Engineering, 191*, 2–9.

Mishra, S., Meena, H., Parashar, V., Khetwal, A., Chakraborty, V., Matsagar, V., Chandel, P., & Singh, M. (2018). High strain rate response of rocks under dynamic loading using split Hopkinson pressure bar. *Geotechnical and Geological Engineering, 36*(1), 531–549.

Peng, R. D., Xue, D. J., Sun, H. F., & Zhou, H. W. (2019). Characteristics of strong disturbance to rock mass in deep mining. *Journal of the China Coal Society, 44*(5), 1359–1368 (in Chinese).

Qian, Y., Zhao, C., Wei, R., Zhang, R., Huang, L., & Chen, H. G. (2024). Self-initiated static-dynamic state transition behavior and triggering mechanism of strain rockburst using three-dimensional discrete element method. *Underground Space, 16*, 143–163.

Rybacki, E., Reinicke, A., Meier, T., Makasi, M., & Dresen, G. (2015). What controls the mechanical properties of shale rocks? - Part I: Strength and Young's modulus. *Journal of Petroleum Science and Engineering, 135*, 702–722.

Scavia, C. (1995). A method for the study of crack propagation in rock structures. *Géotechnique, 45*(3), 447–463.

Scoble, M., Lizotte, Y., & Paventi, M. (1996). Rock mass damage from blasting: Characterization and impact. *Measurement of blast fragmentation, 1*, 11.

Strickland, F. G., & Ren, N. K. (1980). Use of differential strain curve analysis in predicting in-situ stress state for deep wells. *ARMA US Rock Mechanics/Geomechanics Symposium (pp. ARMA-80)*. ARMA.

Su, G. S., Feng, X. T., Wang, J. H., Jiang, J. Q., & Hu, L. H. (2017). Engineering R. Experimental study of remotely triggered rockburst induced by a tunnel axial dynamic disturbance under true-triaxial conditions. *Rock Mechanics and Rock Engineering, 50*(8), 2207–2226.

Waqar, M. F., Guo, S. F., & Qi, S. J. (2023). A comprehensive review of mechanisms, predictive techniques, and control strategies of rockburst. *Applied Sciences, 13*(6), 3950.

Xia, K. W., & Yao, W. (2015). Dynamic rock tests using split Hopkinson (Kolsky) bar system a review. *Journal of Rock Mechanics and Geotechnical Engineering, 7*(1), 27–59.

Xie, H. P., Zhu, J. B., Zhou, T., Zhang, K., & Zhou, C. T. (2020). Conceptualization and preliminary study of engineering disturbed rock dynamics. *Geomechanics and Geophysics for Geo-Energy and Geo-Resources, 6*(2), 1–14.

Xie, H. P., Zhang, K., Zhou, C. T., Wang, J. X., Peng, Q., Guo, J., & Zhu, J. B. (2022). Dynamic response of rock mass subjected to blasting disturbance during tunnel shaft excavation: A field study. *Geomechanics and Geophysics for Geo-Energy and Geo-Resources, 8*(2), 52.

Zhang, C. Q., Feng, X. T., & Zhou, H. (2012). Estimation of in situ stress along deep tunnels buried in complex geological conditions. *International Journal of Rock Mechanics and Mining Sciences, 52*, 139–162.

Zhang, Q. B., & Zhao, J. (2014). A review of dynamic experimental techniques and mechanical behaviour of rock materials. *Rock Mechanics and Rock Engineering, 47*(4), 1411–1478.

Zhou, Z. L., Li, X. B., Ye, Z. Y., & Liu, K. (2010). Obtaining constitutive relationship for rate-dependent rock in SHPB tests. *Rock Mechanics and Rock Engineering, 43*(6), 697–706.